Article

Developmental Cell

Systemic Organ Wasting Induced by Localized Expression of the Secreted Insulin/IGF Antagonist *ImpL2*

Graphical Abstract

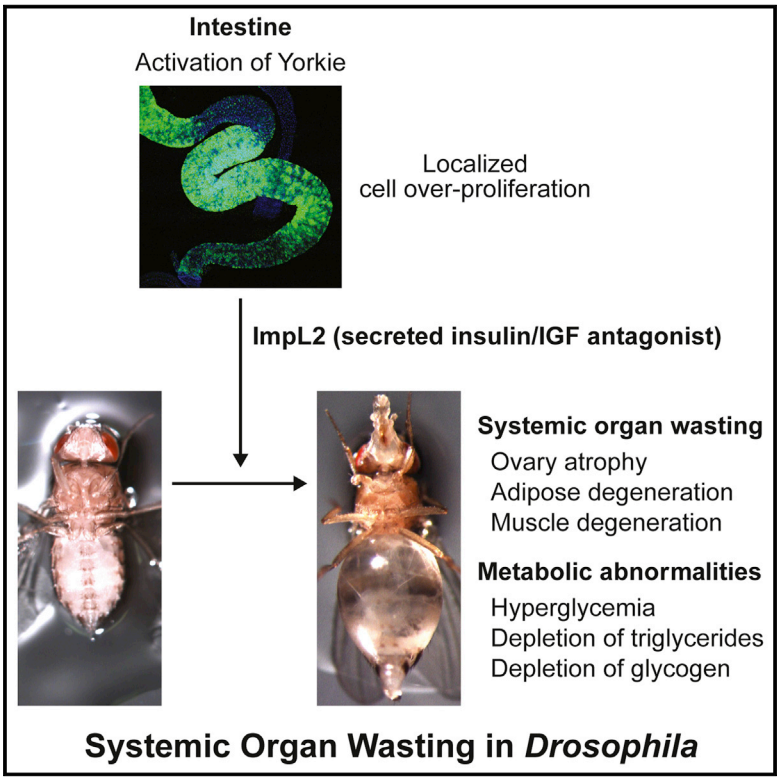

Highlights

- Localized Yki-induced overproliferation causes systemic organ wasting in *Drosophila*
- The secreted insulin/IGF antagonist ImpL2 is a mediator of systemic organ wasting
- ImpL2, secreted from overproliferating tissue, reduces systemic insulin/IGF signaling
- Overproliferating tissue evades wasting via local elevation of insulin/IGF signaling

Authors

Young Kwon, Wei Song, ...,
John M. Asara, Norbert Perrimon

Correspondence

ykwon@genetics.med.harvard.edu (Y.K.),
perrimon@receptor.med.harvard.edu
(N.P.)

In Brief

Wasting is a process characterized by an involuntary loss of body mass observed under diverse conditions, including cancers. Kwon et al. demonstrate that localized Yorkie-induced overproliferation causes systemic organ wasting via the secreted insulin/IGF antagonist ImpL2. These findings establish a model for systemic organ wasting in adult *Drosophila*.

Accession Numbers

GSE65325

Kwon et al., 2015, Developmental Cell *33*, 36–46
April 6, 2015
http://dx.doi.org/10.1016/j.devcel.2015.02.012

CellPress

Developmental Cell
Article

Systemic Organ Wasting Induced by Localized Expression of the Secreted Insulin/IGF Antagonist *ImpL2*

Young Kwon,[1,*] Wei Song,[1] Ilia A. Droujinine,[1] Yanhui Hu,[1] John M. Asara,[3,4] and Norbert Perrimon[1,2,*]
[1]Department of Genetics, Harvard Medical School, Boston, MA 02115, USA
[2]Howard Hughes Medical Institute, Harvard Medical School, Boston, MA 02115, USA
[3]Department of Medicine, Harvard Medical School, Boston, MA 02115, USA
[4]Division of Signal Transduction, Beth Israel Deaconess Medical Center, Boston, MA 02115, USA
*Correspondence: ykwon@genetics.med.harvard.edu (Y.K.), perrimon@receptor.med.harvard.edu (N.P.)
http://dx.doi.org/10.1016/j.devcel.2015.02.012

SUMMARY

Organ wasting, related to changes in nutrition and metabolic activity of cells and tissues, is observed under conditions of starvation and in the context of diseases, including cancers. We have developed a model for organ wasting in adult *Drosophila*, whereby overproliferation induced by activation of Yorkie, the Yap1 oncogene ortholog, in intestinal stem cells leads to wasting of the ovary, fat body, and muscle. These organ-wasting phenotypes are associated with a reduction in systemic insulin/IGF signaling due to increased expression of the secreted insulin/IGF antagonist *ImpL2* from the overproliferating gut. Strikingly, expression of rate-limiting glycolytic enzymes and central components of the insulin/IGF pathway is upregulated with activation of Yorkie in the gut, which may provide a mechanism for this overproliferating tissue to evade the effect of ImpL2. Altogether, our study provides insights into the mechanisms underlying organ-wasting phenotypes in *Drosophila* and how overproliferating tissues adapt to global changes in metabolism.

INTRODUCTION

Wasting is the process characterized by an involuntary loss of body mass manifested in particular by degeneration of skeletal muscles and adipose tissues. Wasting is not only a physiological condition responding to extremely low energy intake and infection but also part of a complex systemic disorder associated with many diseases, including cancers, chronic obstructive lung disease, congestive heart failure, chronic kidney disease, and other chronic diseases (Deboer, 2009; Delano and Moldawer, 2006; Planté-Bordeneuve and Said, 2011; Tisdale, 1997). In particular, 50% of advanced cancer patients are affected by wasting syndrome, which accounts for approximately 20% of cancer death (Fearon et al., 2013; Penna et al., 2010). A number of studies have implicated proinflammatory cytokines, such as tumor necrosis factor α and interleukin 1 and 6, as secreted factors involved in wasting associated with various conditions (Fearon et al., 2013; Kir et al., 2014; Penna et al., 2010; Tisdale, 2009). Additionally, insulin-like growth factor 1 (IGF-1) signaling is a critical regulator of muscle mass maintenance (Bodine et al., 2001; Rommel et al., 2001; Sandri et al., 2004). Downregulation of IGF-1 signaling in skeletal muscles decreases Akt activity and in turn increases Foxo activity, which induces muscle protein degradation through the ubiquitin-proteasome system and autophagy (Han et al., 2013). Moreover, the transforming growth factor β family members myostatin and activin have been identified as additional secreted factors regulating organ wasting (Fearon et al., 2012; Han et al., 2013). Stimulation of myostatin/activin signaling in skeletal muscles activates Smad2/3 signaling and inhibits Akt signaling, which increases catabolism of muscle proteins (Fearon et al., 2012; Han et al., 2013).

The "bloating syndrome," observed in flies transplanted with imaginal discs mutant for the tumor suppressor *lethal (2) giant larvae* (*l(2)gl*) (Gateff and Schneiderman, 1974), is a systemic phenotype relevant to the wasting syndrome. Whereas a wild-type imaginal disc transplanted into the abdomen of an adult fly only grows until it reaches its normal size, a transplanted *l(2) gl* mutant disc undergoes neoplastic growth and eventually kills the fly. However, before they die, these flies develop the bloating syndrome, whereby the abdomen becomes swollen and translucent and the fat body and ovaries are almost completely degenerated (Gateff and Schneiderman, 1974). This degeneration of the fat body and ovaries is reminiscent of the wasting of adipose tissue and skeletal muscles in mammals, because the fat body and ovaries are the organs preserving energy in the forms of lipids and proteins in *Drosophila*. Strikingly, although the bloating syndrome is a robust phenotype, it has not been characterized in detail. In particular, it is not known whether the wasting process affects metabolism and how neoplastic *l(2)gl* mutant discs induce degeneration of ovaries and the fat body.

The transcriptional coactivator *yorkie* (*yki*) regulates growth, repair, and regeneration by inducing a transcriptional program required for cell proliferation and survival (Halder and Johnson, 2011; Harvey and Hariharan, 2012; Pan, 2010; Staley and Irvine, 2012; Yang and Xu, 2011). In particular, studies in adult *Drosophila* have identified a crucial role of *yki* in the regulation of intestinal stem cell (ISC) proliferation during tissue

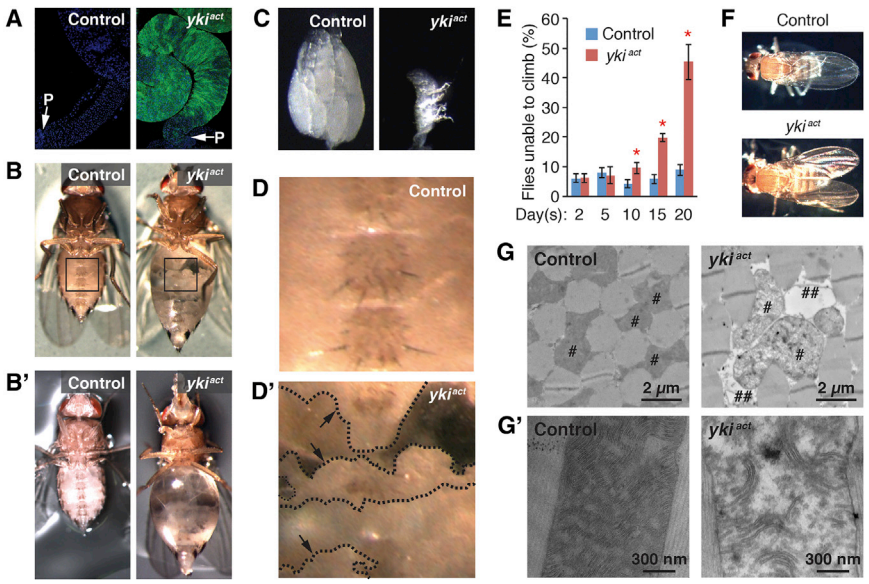

Figure 1. Degeneration of Ovary, Fat Body, and Muscle in $esg^{ts}>yki^{act}$ Flies

(A) Midgut images. GFP is driven by esg^{ts} (*esg-GAL4*, *tub-GAL80^{ts}*, *UAS-GFP*/+). The arrows indicate the posterior (P) end of the midgut.

(B and B′) Fly images. Transgenes were induced for 6 days (B) and 12 days (B′) with esg^{ts}.

(C) Ovary images. Transgenes were induced for 8 days.

(D and D′) Magnified views of the insets in (B). The dashed lines and arrows indicate the boundary of the fat body.

(E) Quantification of climbing defects (mean ± SEMs). *$p \leq 0.05$, Student's t test.

(F) Downturned wing phenotype in $esg^{ts}>yki^{act}$ flies.

(G) Electron microscopic images of the transverse section of indirect flight muscles. #, mitochondria; ##, empty spaces.

(G′) Images of mitochondrion. In all muscle experiments, transgenes were induced for 20 days in male flies unless otherwise indicated. The genotype of control is *esg-GAL4*, *tub-GAL80^{ts}*, *UAS-GFP*/+ and yki^{act} is *esg-GAL4*, *tub-GAL80^{ts}*, *UAS-GFP*/+; *UAS-yki^{act}*/+.

homeostasis and damage (Karpowicz et al., 2010; Ren et al., 2010; Shaw et al., 2010). Furthermore, these studies have shown that activation of Yki in the midgut induces massive cell proliferation, which conceivably affects the physiology of the proliferating tissue as well as the homeostasis of distant tissues and the whole organism. However, it is not known whether and how localized cell proliferation in the midgut driven by activation of Yki perturbs the physiology and function of distant organs and the whole organism.

Here we show that induction of aberrant cell proliferation in the midgut by activation of Yki causes the bloating syndrome, which is associated with degeneration of the ovary, fat body, and muscle. We characterize in detail the systemic wasting phenotypes associated with the proliferating midgut using genomic, metabolomic, and physiological analyses. Finally, we show that the secreted insulin/IGF antagonist *ImpL2* is involved in the wasting process by decreasing systemic insulin/IGF signaling.

RESULTS

Localized Aberrant Cell Proliferation Induced by Activation of Yki in ISCs Causes Systemic Organ Wasting

To address how localized aberrant cell proliferation alters organismal homeostasis, we expressed an active form of *yki* (yki^{act}) (Oh and Irvine, 2009) in adult midgut ISCs using the conditional GAL4 driver esg^{ts} (*esg-GAL4*, *tub-GAL80^{ts}*, *UAS-GFP*/+) (hereafter referred to as $esg^{ts}>yki^{act}$). Consistent with the proposed role of *yki* in the midgut (Karpowicz et al., 2010; Ren et al., 2010; Shaw et al., 2010), expression of yki^{act} resulted in massive cell proliferation as detected by an increase in GFP signal and aberrant shape of the gut (Figure 1A). Strikingly, over time, these flies developed the bloating syndrome phenotype (Figures 1B and B′), originally described in adult flies with transplanted imaginal discs harboring a mutation in the tumor suppressor *l(2)gl* in the abdomen (Gateff and Schneiderman, 1974). $esg^{ts}>yki^{act}$ flies exhibit this bloating phenotype as early as 5 days after induction of yki^{act}. Both the penetrance and severity of the phenotype progressively increase, with ~70% of flies showing the phenotype at 6 days (Figure 1B) and ~95% at 12 days (Figure 1B′). Additionally, ovaries and fat bodies of $esg^{ts}>yki^{act}$ females degenerate progressively with time (Figures 1C and 1D). In adult flies, the fat body does not form as a discrete structure but fills the abdominal space, resulting in a continuous light yellow mass. Whereas fat bodies in controls were not affected (Figures 1B and 1D), the fat bodies in $esg^{ts}>yki^{act}$ flies were observed as discontinuous patches at 6 days (Figures 1B and 1D′) and were almost completely degenerated at 12 days of yki^{act} induction (Figure 1B′; magnified images are not shown). Furthermore, we observed accelerated decline of muscle function in $esg^{ts}>yki^{act}$ flies. $esg^{ts}>yki^{act}$ flies showed progressive climbing defects (Figure 1E) and downturned wings (Figure 1F), general indicators of muscle weakening/degeneration (Demontis and Perrimon, 2010; Greene et al., 2003). To characterize the underlying cellular defects associated with muscle weakening/degeneration in $esg^{ts}>yki^{act}$, we examined the structures of $esg^{ts}>yki^{act}$ muscles by electron microscopy. Mitochondria of $esg^{ts}>yki^{act}$ muscles were swollen and often associated with empty space (Figure 1G). Moreover, cristae were fragmented, and inner mitochondrial space was filled with low-electron-dense sectors (Figure 1G′), indicative of mitochondrial degeneration (Greene et al., 2003). Altogether, these findings reveal that aberrant cell proliferation induced by activation of Yki in ISCs causes systemic organ-wasting phenotypes affecting ovaries, fat body, and muscle.

Expression of yki^{act} in Midgut Causes Repression of Genes Involved in Energy Metabolism in Muscle

To gain insight into the systemic phenotypes induced by $esg^{ts}>yki^{act}$, we performed a transcriptomic analysis of thoracic muscles (Table S1), which play an important role in the regulation

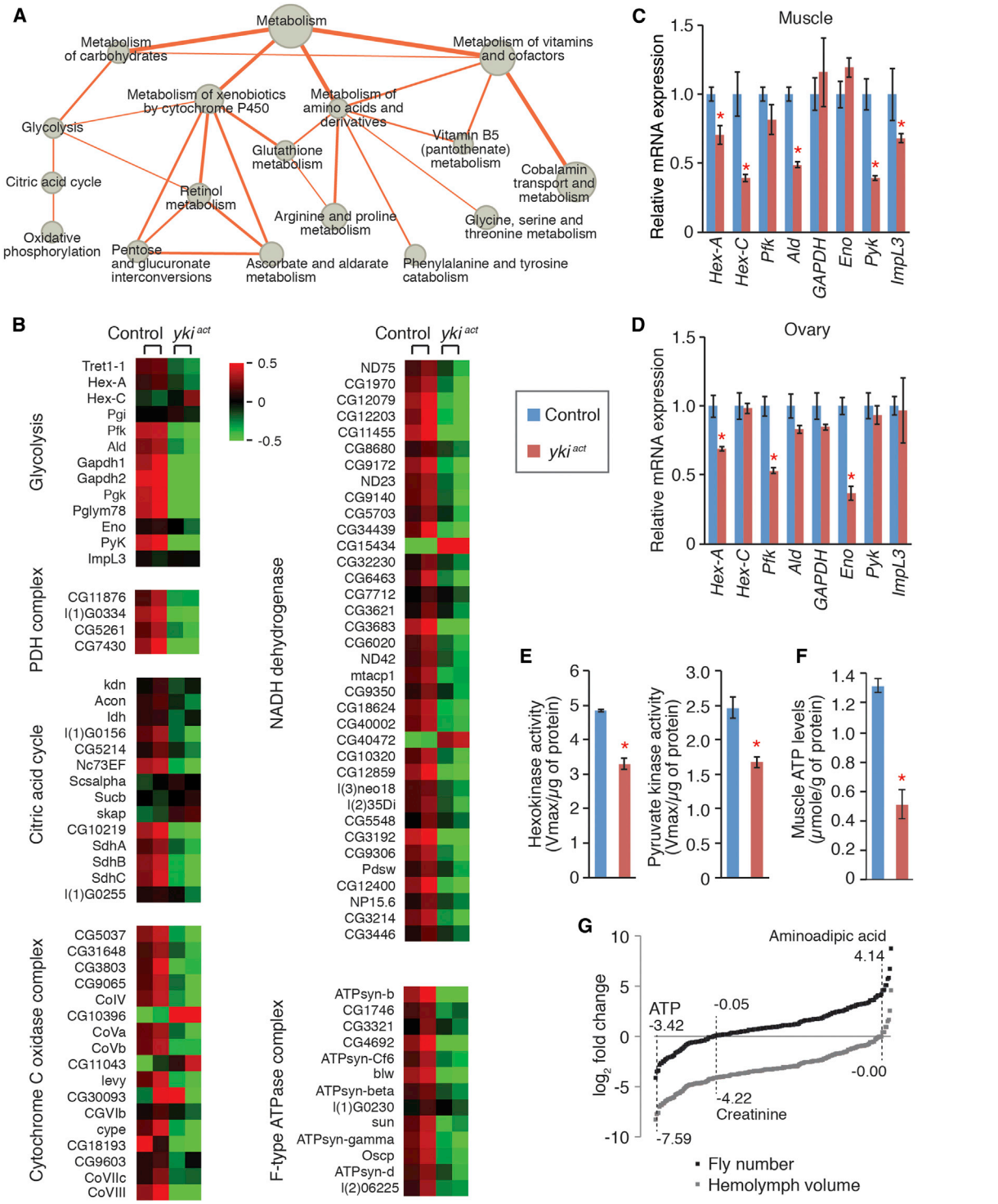

Figure 2. Repression of Energy Metabolism in *esg^{ts}>yki^{act}* Muscles

(A) Network presentation of gene list enrichment analysis results focusing on metabolism. All presented metabolic processes are identified to be significantly downregulated in muscles of *esg^{ts}>yki^{act}* flies (Tables S2 and S3). Node size indicates enrichment ($-\log_{100}$ p value), and edge thickness represents the number of common genes between two gene sets. The citric acid cycle and pyruvate metabolism (p = 0.0253, GSEA) and oxidative phosphorylation (p = 0.000, GSEA) are identified by GSEA analysis (Subramanian et al., 2005).

(B) Representative downregulated processes and complexes involved in energy metabolism. Heat map signal indicates $\log_2$ fold-change values relative to the mean expression level within the group. Red signal denotes higher expression and green signal denotes lower expression relative to the mean expression level within the group. Related GSEA plots are shown in Figure S1.

(legend continued on next page)

of organismal physiology and aging by affecting systemic insulin/IGF signaling and trehalose/glucose metabolism (Demontis and Perrimon, 2010). Interestingly, gene list enrichment analysis of the downregulated muscle transcriptome revealed a striking enrichment of multiple metabolic processes impinging on carbohydrate metabolism ($p = 0.0018$), amino acid metabolism ($p = 1.32 \times 10^{-7}$), metabolism of vitamins and cofactors ($p = 1.32 \times 10^{-7}$), and metabolism of xenobiotics by cytochrome P450 ($p = 1.45 \times 10^{-4}$) (Figure 2A; Tables S2 and S3). Furthermore, we found a systematic repression of genes involved in energy metabolism ($p = 0.000$, gene set enrichment analysis; GSEA), including glycolysis ($p = 0.018$, GSEA), pyruvate metabolism and the citric acid cycle ($p = 0.0252$, GSEA), and oxidative phosphorylation ($p = 0.000$, GSEA) (Figures 2A and 2B; Figure S1; Table S4). We further confirmed by quantitative (q)PCR that the expression of multiple genes involved in glycolysis was decreased not only in muscles but also in ovaries of $esg^{ts}>yki^{act}$ flies (Figures 2C and 2D). Moreover, the activities of the two rate-limiting glycolytic enzymes Hexokinase (Hex-A and Hex-C) and Phosphofructokinase (Pfk) are reduced by approximately 30% in $esg^{ts}>yki^{act}$ muscle (Figure 2E). Accordingly, ATP levels in muscles were significantly decreased in $esg^{ts}>yki^{act}$ flies as compared to controls (Figure 2F). Moreover, metabolomic analyses revealed a decrease of ATP, NADH, and NADPH levels in the hemolymph of $esg^{ts}>yki^{act}$ flies (Figure 2G; Figure S2; Table S5), which are the main products of energy metabolism. Altogether, these results suggest that $esg^{ts}>yki^{act}$ alters the metabolic gene expression program of distant tissues, which is manifested by downregulation of genes involved in glycolysis in muscle and ovaries.

Overproliferating Midgut due to Activation of Yki Causes Hyperglycemia

Because we observed that gene expression of glycolytic enzymes in muscles and ovaries was downregulated in $esg^{ts}>yki^{act}$ flies, we investigated whether there were any changes in glucose metabolism in these flies. As expected from the bloating phenotype, the volume of extractable hemolymph from $esg^{ts}>yki^{act}$ flies was greatly increased as compared to controls (Figure 3A). Nevertheless, the concentration of trehalose, the primary circulating sugar composed of two alpha-glucoses, was significantly increased in the hemolymph of $esg^{ts}>yki^{act}$ flies (Figure 3B). Accordingly, whole-body trehalose levels were increased in $esg^{ts}>yki^{act}$ flies (Figure 3C). Additionally, consistent with the degeneration of the fat body that stores triglycerides and glycogen in the adult, whole-body triglycerides and glycogen levels were reduced in $esg^{ts}>yki^{act}$ flies, as compared to controls (Figures 3D and 3E).

Starvation causes a reduction in whole-body trehalose levels (Figure S3B), suggesting that the increase of trehalose levels in $esg^{ts}>yki^{act}$ flies is not due to the effect of starvation (Figures 3B and 3C). Nevertheless, starvation affects storage of triglycerides and glycogen (Figures S3C and S3D). Thus, because the presence of cell overproliferation in the midgut could in principle perturb gut functions and mimic starvation, we addressed whether $esg^{ts}>yki^{act}$ altered food intake and absorption. Measurements of food intake and excretion did not appear to be significantly affected in $esg^{ts}>yki^{act}$ flies (Figures 3F and 3G). To further test whether $esg^{ts}>yki^{act}$ flies are starved, we examined *Drosophila* insulin-like peptide 2 (Dilp2) levels in Dilp-producing cells (IPCs) in the brain, because starvation causes accumulation of *Dilp2*, presumably due to a reduction in secretion (Demontis and Perrimon, 2010; Géminard et al., 2009; Ikeya et al., 2002). Surprisingly, the Dilp2 signal in the IPCs of $esg^{ts}>yki^{act}$ flies was significantly decreased (Figures 3H and 3I). This decrease of Dilp2 signal is not due to a reduction in *Dilp2* mRNA, as we observed that the levels of *Dilp* mRNAs in the heads remained unaffected in $esg^{ts}>yki^{act}$ flies (Figure 3J). Moreover, we tested a starvation marker, *Pepck*, which is regulated by both sugar and glycine (Zinke et al., 1999), and found that *Pepck* mRNA expression was increased ~50-fold during starvation (Figure S3F). Conversely, *Pepck* mRNA expression remained unaltered at 6 days of yki^{act} induction and increased ~3-fold at 12 days (Figure S3F), suggesting that $esg^{ts}>yki^{act}$ flies were not severely starved. Altogether, these findings indicate that aberrant cell proliferation, induced by activation of *yki*, causes systemic abnormality in trehalose/glucose metabolism, which resembles hyperglycemia. Further, because Dilp2 is not accumulated in the IPCs and *Pepck* expression is not greatly affected, it is unlikely that starvation is the main cause of the phenotypes associated with $esg^{ts}>yki^{act}$. However, we cannot rule out that other aspects of gut function are perturbed, contributing to the organ-wasting and bloating phenotypes (see Discussion).

Depletion of *ImpL2* from $esg^{ts}>yki^{act}$ Midguts Rescues Systemic Reduction of Akt1 Phosphorylation and Hyperglycemia

To identify the signaling factor(s) impinging on systemic phenotypes in $esg^{ts}>yki^{act}$ flies, we interrogated the muscle transcriptome of $esg^{ts}>yki^{act}$. Interestingly, target genes of Foxo, a transcription factor inhibited by insulin/IGF signaling, are enriched in the upregulated muscle transcriptome of $esg^{ts}>yki^{act}$ flies ($p = 0.039$; Figure 4A). In particular, *Thor* (human 4E-BP ortholog), a well-characterized target of Foxo, is significantly upregulated (Figure 4B). Consistent with the transcriptome analysis results, Akt phosphorylation is significantly reduced in muscles and heads of $esg^{ts}>yki^{act}$ flies (Figure 4C). To characterize the mechanism by which $esg^{ts}>yki^{act}$ reduces systemic insulin/IGF signaling, we examined whether the expression of *ImpL2*, a secreted protein that resembles IGFBP7 (Sloth Andersen et al., 2000) and that inhibits insulin/IGF signaling by forming

(C and D) Relative mRNA expression of glycolytic enzyme in muscle (C) and ovaries (D). Measurements shown are mean ± SDs.

(E) Activities of Hexokinase (left) and Pyruvate kinase (right) in muscle at 8 days of induction (mean ± SEMs).

(F) ATP levels in muscle at 20 days of transgene induction.

(G) Metabolomic analysis of hemolymph metabolites. The metabolite counts are normalized to fly number (black) or extracted hemolymph volume (gray). Log_2 fold-change values of the metabolites in hemolymph of $esg^{ts}>yki^{act}$ flies relative to control are presented.

Reduced 55 metabolites in hemolymph of $esg^{ts}>yki^{act}$ flies are shown in Figure S2. *$p \leq 0.05$ (Student's t test) compared to control. Genotypes are as shown in Figure 1.

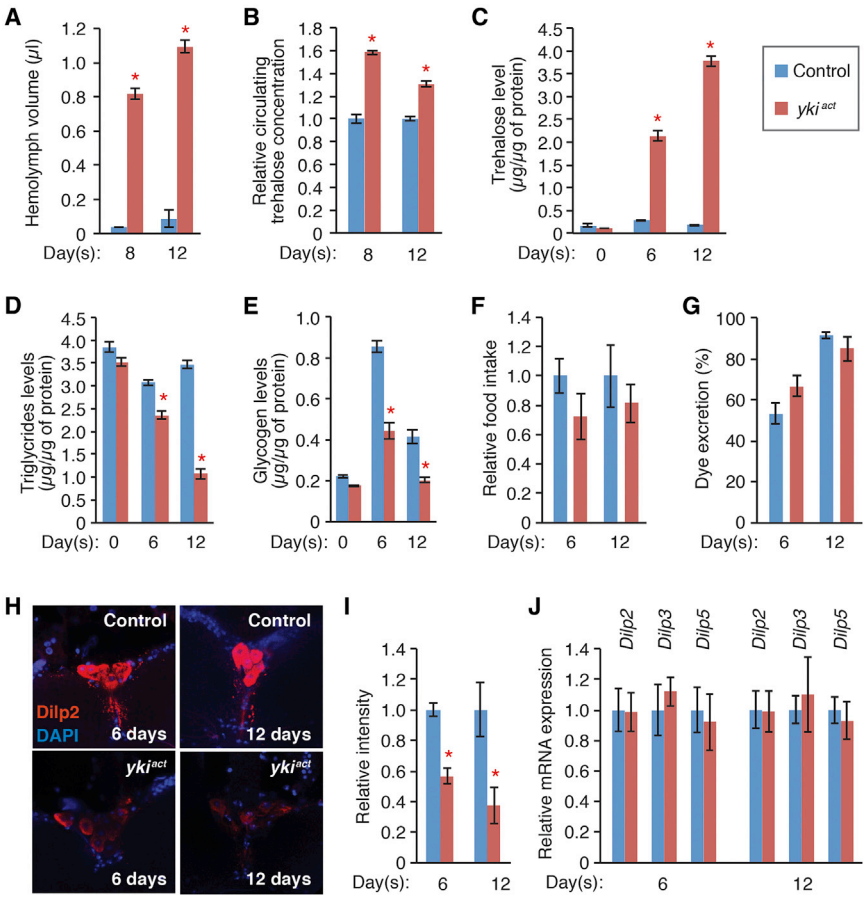

Figure 3. *esg*^{ts}>*yki*^{act} Causes Hyperglycemia and Depletion of Triglycerides and Glycogen

(A) Volumes of extractable hemolymph per fly after 8 and 12 days of induction with *esg*^{ts}.

(B) Relative concentration of circulating trehalose normalized to control at 8 and 12 days of induction.

(C) Trehalose levels in whole flies normalized to extracted protein amounts at different induction times.

(D) Triglyceride levels in whole flies. Triglyceride levels were normalized to protein amounts.

(E) Glycogen levels in whole flies. Glycogen levels were normalized to protein amounts.

(F) Food intake measured by CAFE assay (Demontis and Perrimon, 2010; Ja et al., 2007) after 6 and 12 days of transgene induction with *esg*^{ts}. Values relative to controls are presented.

(G) Food excretion rate. Transgenes are induced for 6 and 12 days. The percentages of excreted dye amount to total intake are shown.

(H) Dilp2 staining in the IPCs in the brain. Images are captured with the same confocal setting.

(I) Quantification of Dilp2 signal intensity in IPCs. Dilp2 signals are normalized to background signals, and values relative to controls are presented.

(J) mRNA levels in the heads measured by qPCR. The results shown in (A)–(E) are mean ± SEMs. The values in (F), (G), (I), and (J) are mean ± SDs. *p ≤ 0.05 (Student's t test) compared to control. Genotypes are as shown in Figure 1.

a protein complex with circulating Dilps (Alic et al., 2011; Honegger et al., 2008), was affected in *esg*^{ts}>*yki*^{act} flies. Strikingly, *ImpL2* mRNA expression was greatly elevated in *esg*^{ts}>*yki*^{act} midguts at 6 days of *yki*^{act} induction, whereas the expression of *ImpL2* remained unchanged in muscles, ovaries, heads, and fat bodies (Figure 4D). Interestingly, starvation regulates *ImpL2* expression (Honegger et al., 2008), and we further confirmed that starvation increased *ImpL2* mRNA expression in heads, muscles, midguts, and fat bodies (Figure S3E). The absence of *ImpL2* mRNA induction in the muscles, ovaries, heads, and fat bodies of *esg*^{ts}>*yki*^{act} flies further supports that these flies are not calorie deprived. Moreover, *ImpL2* mRNA expression is increased ~70-fold in the *esg*^{ts}>*yki*^{act} midgut, which appears to greatly exceed the range of induction during starvation (Figure 4D; Figure S3E).

To address the role of *ImpL2*, we examined whether removal of *ImpL2* activity could rescue the systemic phenotypes associated with *esg*^{ts}>*yki*^{act}. The null allele *ImpL2*^{Def20} (Honegger et al., 2008) completely rescued the reduction of Akt1 phosphorylation in *esg*^{ts}>*yki*^{act} flies (Figure 4C) and restored circulating trehalose concentration and whole-body trehalose levels (Figures S4A and S4B). The rescue of the systemic phenotypes associated with *esg*^{ts}>*yki*^{act} by *ImpL2*^{Def20} is presumably due to a systemic increase of insulin/IGF signaling, as *ImpL2*^{Def20} alone caused a slight increase of Akt1 phosphorylation (Figure 4C) and reduction of circulating trehalose concentration (Figure S4A). Next, to examine the importance of *ImpL2* induction in the midgut, we coexpressed an RNAi against *ImpL2* (*15009R-3*) together with *yki*^{act}. The expression of *ImpL2*-RNAi efficiently suppressed the induction of *ImpL2* in *esg*^{ts}>*yki*^{act} midgut (~80% knockdown efficiency), although the expression of *ImpL2* remained 8-fold higher than in controls (Figure S4C). Notably, expression of *ImpL2*-RNAi alone using *esg*^{ts} did not significantly alter Akt1 phosphorylation and trehalose levels (Figures 4C, 4E, and 4F). Importantly, knockdown of *ImpL2* with *esg*^{ts} restored Akt1 phosphorylation in muscles and heads significantly (Figure 4C) and reduced the trehalose levels (Figures 4E and 4F). This rescue is not due to suppression of cell proliferation, because the overall shape and GFP intensity of *esg*^{ts}>*yki*^{act} midguts remained unaltered after *ImpL2*-RNAi expression (Figure 4G). Additionally, similar experiments employing an additional *ImpL2*-RNAi line (*30931*) further confirmed the importance of *ImpL2* induction in the midgut for the systemic phenotypes associated with *esg*^{ts}>*yki*^{act} (Figures S4D–S4F). In addition, ectopic expression of *ImpL2* in enterocytes (ECs) in the midgut caused hyperglycemia, reduction of Akt1 phosphorylation in muscle, increase of hemolymph volume, and ovary atrophy (Figures S4G–S4K), suggesting that the increased *ImpL2* expression was sufficient to cause some of the systemic phenotypes associated with *esg*^{ts}>*yki*^{act}. Altogether, our results indicate that induction of *ImpL2* in *esg*^{ts}>*yki*^{act} midguts is a critical determinant for both the hyperglycemia and systemic reduction of insulin/IGF signaling in *esg*^{ts}>*yki*^{act} flies.

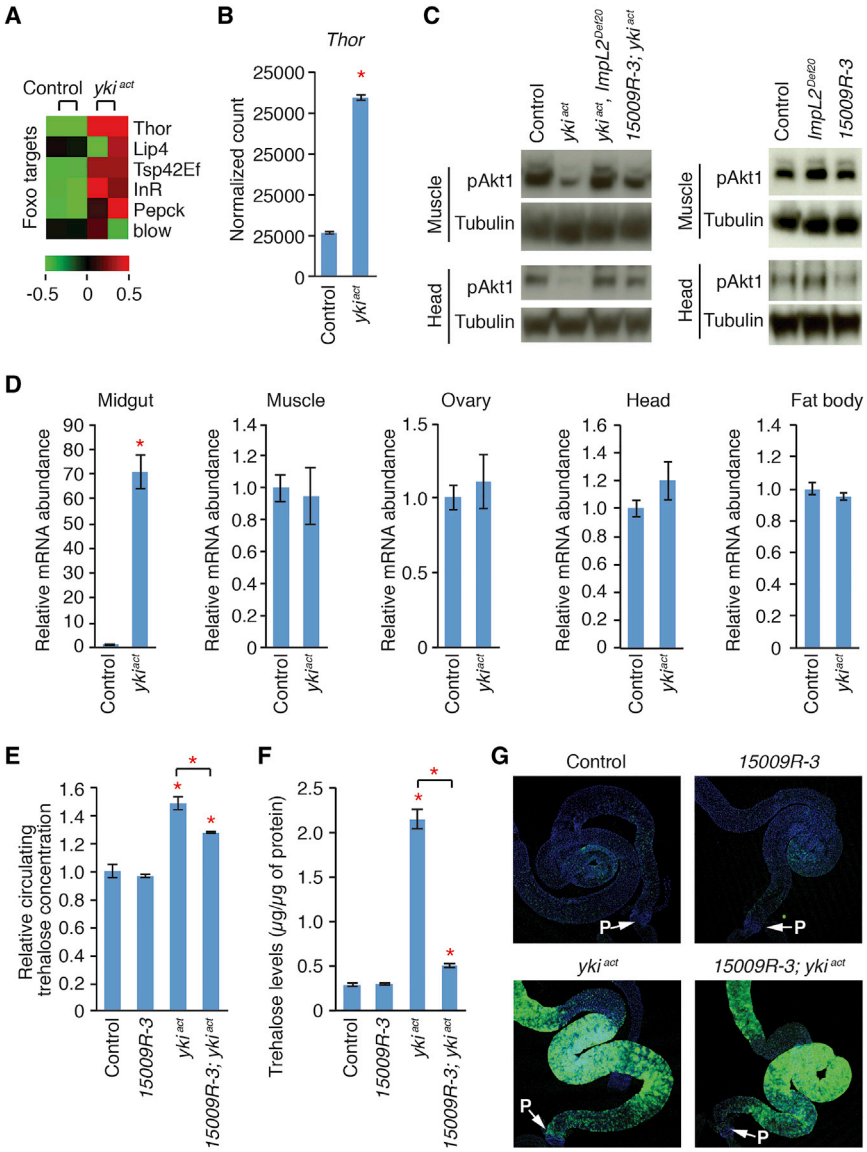

Figure 4. Depletion of *ImpL2* from *esg^{ts}>yki^{act}* Midgut Rescues Systemic Reduction of Insulin/IGF Signaling and Hyperglycemia

(A) Heat map showing expression of the Foxo target gene set. Foxo target genes are annotated from DroID (Murali et al., 2011).

(B) Normalized expression levels of *Thor* (human 4E-BP ortholog). The values shown are mean ± SEMs. The asterisk denotes statistically significant difference from control (adjusted $p = 1.239 \times 10^{-87}$; p values are adjusted with the Benjamini-Hochberg procedure, which controls the false discovery rate; Benjamini and Hochberg, 1995).

(C) Akt1 phosphorylation in muscle and head at 8 days of induction.

(D) Relative expression levels of *ImpL2* mRNA in the midgut, muscle, ovary, head, and fat body. The active form of *yki* (*yki^{act}*) was expressed in the midgut with *esg^{ts}* for 6 days. The values are mean ± SDs. *$p < 0.05$, unpaired Student's t test.

(E) Circulating trehalose concentrations at 8 days of induction.

(F) Trehalose levels in the whole-body void at 6 days of induction. The measurements are normalized to total protein amounts.

The results shown in (E) and (F) are mean ± SEMs. *$p \leq 0.05$ (Student's t test) compared to control other than when indicated by a bracket.

(G) Midgut morphology. GFP is driven by *esg^{ts}* and *UAS-GFP*. Nuclei are marked with 4′,6-diamidino-2-phenylindole (DAPI) (blue). The arrows indicate the posterior end of the midgut. The genotype of control is *esg-GAL4*, *tub-GAL80^{ts}*, *UAS-GFP/+*, *yki^{act}* is *esg-GAL4*, *tub-GAL80^{ts}*, *UAS-GFP/+*; *UAS-yki^{act}/+*, *yki^{act}*, *ImpL2^{Def20}* is *esg-GAL4*, *tub-GAL80^{ts}*, *UAS-GFP/+*; *UAS-yki^{act}*, *ImpL2^{Def20}/ImpL2^{Def20}*, *15009R-3* is *esg-GAL4*, *tub-GAL80^{ts}*, *UAS-GFP/15009R-3* (*UAS-ImpL2* RNAi from the National Institute of Genetics, Japan), *15009R-3; yki^{act}* is *esg-GAL4*, *tub-GAL80^{ts}*, *UAS-GFP/15009R-3*; *UAS-yki^{act}/+*, and *ImpL2^{Def20}* is *esg-GAL4*, *tub-GAL80^{ts}*, *UAS-GFP/+*; *ImpL2^{Def20}/ImpL2^{Def20}*.

Depletion of *ImpL2* in *esg^{ts}>yki^{act}* Midguts Rescues Ovary Wasting and Muscle Degeneration

Next, we addressed whether *ImpL2* is involved in the organ-wasting process associated with *esg^{ts}>yki^{act}*. Interestingly, either *ImpL2^{def20}* or depletion of *ImpL2* in the midgut with *esg^{ts}* suppressed wasting of ovaries caused by *esg^{ts}>yki^{act}* (Figure 5A). In addition, expression of *ImpL2* in the midgut is required for the muscle degeneration observed in *esg^{ts}>yki^{act}* flies. Depletion of *ImpL2* in the midgut with *esg^{ts}* rescued the climbing defects and downturned wings in *esg^{ts}>yki^{act}* flies (Figures 1E, 1F, 5B, and 5C). Strikingly, expression of *ImpL2*-RNAi with *esg^{ts}* was sufficient to significantly rescue the mitochondrial defects (Figures 1G, 1G′, 5D, and 5D′) and reduced ATP levels (Figures 2F and 5E). Finally, we found that the bloating phenotype in *esg^{ts}>yki^{act}* flies was also dependent on *ImpL2*, because knockdown of *ImpL2* in the midgut with *esg^{ts}* significantly rescued the bloating phenotype (Figure 5F). Altogether, these results indicate that degeneration of ovaries and muscle in *esg^{ts}>yki^{act}* flies is dependent on increased expression of *ImpL2* in the midgut.

Expression of Insulin/IGF Pathway Components and Glycolytic Enzymes Is Upregulated in the Proliferating Midgut due to Aberrant Activation of Yki

Although insulin/IGF signaling is indispensable for *yki^{act}*-mediated cell proliferation in the midgut (data not shown), *esg^{ts}>yki^{act}* midguts undergo cell proliferation irrespective of the induction of *ImpL2*. Strikingly, instead of observing a reduction of Akt1 phosphorylation, expression of *yki^{act}* increased the levels of both pAkt1 and Akt1 in the midgut (Figures 6A and 6B), similar to a previous observation in the wing disc (Ye et al., 2012). Moreover, overall Akt1 phosphorylation in the midgut was greatly increased as compared to control (Figure S5). Interestingly, we found that gene expression of insulin/IGF pathway components was systematically increased

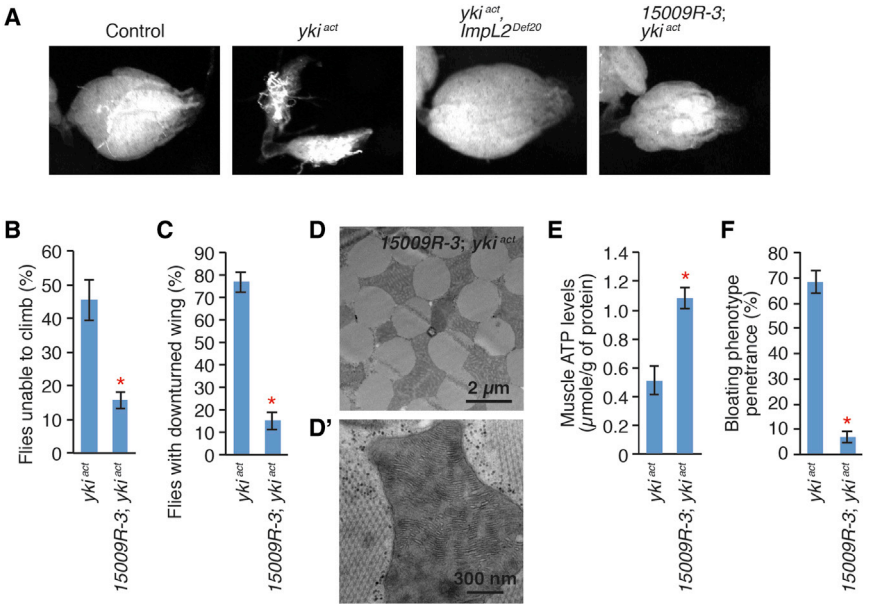

Figure 5. Depletion of *ImpL2* with *esg*^{ts} Rescues Degeneration of Ovaries and Muscle Associated with *esg*^{ts}>*yki*^{act}

(A) Images of ovaries from the indicated genotypes. Transgenes are induced for 8 days with *esg*^{ts}.

(B) Quantification of climbing defect.

(C) Penetrance of downturned wing phenotype.

(D) Electron microscopic image of transverse section of indirect flight muscles.

(D′) Image of mitochondrion.

(E) Muscle ATP levels normalized to protein levels. In all muscle experiments, transgenes are induced for 20 days in male flies.

(F) Penetrance of the bloating syndrome at 8 days of transgene induction. Either control (*esg*^{ts}) or expression of *15009R-3* alone with *esg*^{ts} is not associated with the bloating syndrome phenotype.

All quantifications shown are mean ± SEMs. *p ≤ 0.05, Student's t test compared to *yki*^{act}. Genotypes are as shown in Figure 4.

in *esg*^{ts}>*yki*^{act} midgut (*InR*, ~8-fold; *Akt1*, ~12-fold; Figure 6C). Conversely, the mRNA levels of these genes were not affected significantly in muscles and ovaries, with the exception of *InR* in muscles (Figure S6). Finally, expression of *yki*^{act} in the midgut elevated the transcript of *Dilp3*, which regulates insulin/IGF signaling in that tissue (O'Brien et al., 2011) (Figure 6D). Thus, our findings suggest that expression of *yki*^{act} in the midgut causes a disparity in the activity of insulin/IGF signaling between the midgut and other tissues. Interestingly, extracellular signal-regulated kinase activation was shown to enhance insulin/IGF signaling by increasing the expression of *InR* transcript (Zhang et al., 2011). Additionally, *ras*^{V12}; *csk*$^{-/-}$ transformed cells increased *InR* expression through Wingless signaling to evade the insulin resistance induced by a high-sugar diet (Hirabayashi et al., 2013). Although Foxo is a well-characterized transcription factor regulating *InR* expression (Puig and Tjian, 2005), these observations and ours suggest that some mitogenic signals can enhance insulin/IGF signaling by increasing *InR* expression.

This disparity of insulin/IGF signaling activities presumably leads to differential regulation of glucose metabolism between the midgut and other tissues. In contrast to the observations in muscles and ovaries (Figures 2C and 2D), the mRNA expression of glycolytic enzymes was systematically increased in *esg*^{ts}>*yki*^{act} midguts (Figure 6E). In particular, the mRNA levels of two key rate-limiting enzymes, *Hex-A* and *Pfk*, were increased by ~4- and ~10-fold, respectively, and the ortholog of lactate dehydrogenase, *ImpL3*, which is a major contributor to the Warburg effect (Vander Heiden et al., 2009; Warburg, 1956), was increased ~7-fold. Consistent with overproliferation in the midgut, we observed increased glucose incorporation in *esg*^{ts}>*yki*^{act} midgut as compared to controls (Figure 6F). Strikingly, in other parts of these flies, glucose incorporation was reduced by ~50% (Figure 6F), a process dependent on wild-type *ImpL2* allele, because *ImpL2*^{def20} rescued the reduction of glucose incorporation in the whole-body void of midgut and hemolymph induced by *esg*^{ts}>*yki*^{act} (Figure 6F). Altogether, these observations suggest that activation of *yki* in the midgut causes a bias in glucose metabolism between the midgut and other tissues, and that *ImpL2* is a genetic determinant of this phenomenon.

DISCUSSION

In this study, we describe the unexpected observation that the overproliferating midgut due to aberrant Yki activity in ISCs induces the bloating syndrome and systemic organ wasting. Additionally, the overproliferating midgut perturbs organismal metabolism, resulting in an increase of hemolymph trehalose and depletion of glycogen and triglyceride storage (Figure 7). Strikingly, we show that the accumulation of hemolymph trehalose and organ-wasting processes are dependent on the antagonist of insulin/IGF signaling, *ImpL2*, which is specifically upregulated in the proliferating midgut. Our study provides strong genetic evidence supporting that systemic organ wasting associated with the aberrant activation of Yki in ISCs cannot be explained solely by the perturbation of general gut function. Based on these findings, we propose that *ImpL2* is a critical factor involved in systemic organ wasting in *Drosophila*.

In an accompanying paper in this issue of *Developmental Cell*, Figueroa-Clarevega and Bilder show that transplantation of *scrib*^{1}/*Ras*^{V12} disc tumors into wild-type flies induces the bloating syndrome phenotype and systemic organ wasting, affecting ovaries, fat bodies, and muscles (Figueroa-Clarevega and Bilder, 2015). Figueroa-Clarevega and Bilder also identify *ImpL2* as a tumor-driven factor that plays a critical role in the organ-wasting process. These results are consistent with our findings and indicate that the bloating syndrome and organ-wasting phenotypes are not associated specifically with perturbation of gut function. Interestingly, Figueroa-Clarevega and Bilder observe that disc tumors derived by the expression of *yki*$^{S/A}$ (an active form of *yki* that is less potent than *yki*^{act} used in this study) did not cause organ wasting, which can be explained by the low level

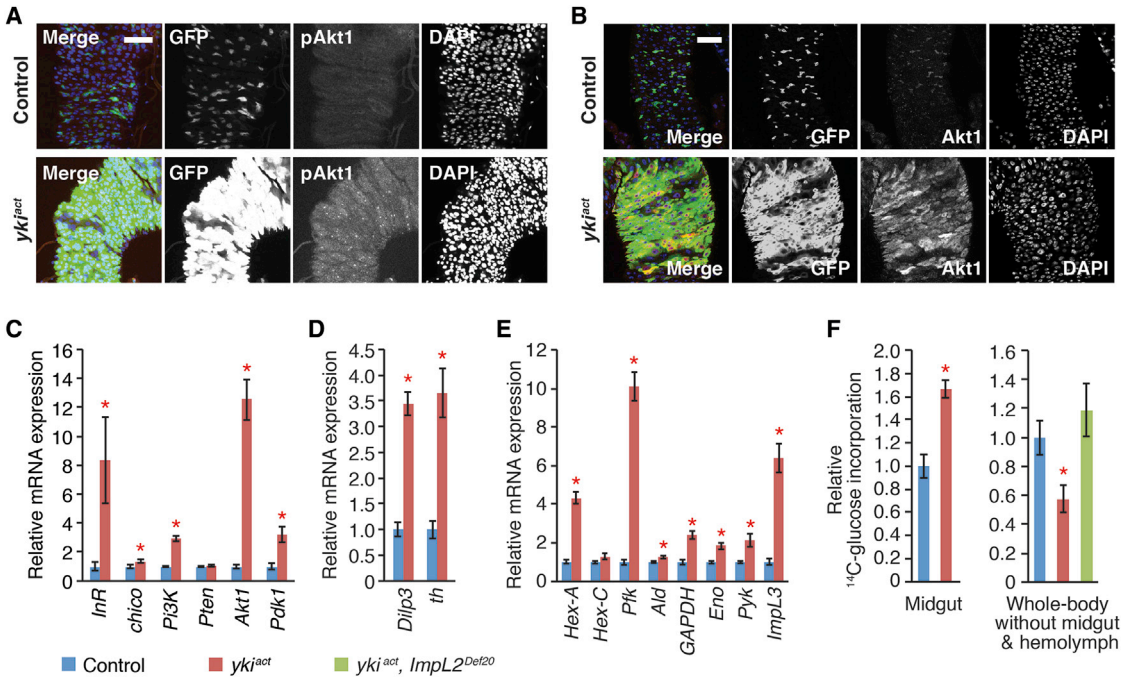

Figure 6. Upregulation of Insulin/IGF Signaling in *esg*^{ts}>*yki*^{act} Midguts

(A and B) Both phosphorylation of Akt1 (pAkt1; red in merge; A) and expression of Akt1 (red in merge; B) are increased in *esg*^{ts}>*yki*^{act} midguts. Nuclear staining is shown with DAPI (blue in merge). The scale bars represent 50 μm. We characterized anti-Akt and anti-pAkt antibodies in the midgut (Figure S7).

(C) Relative mRNA expression of insulin/IGF pathway components in the midgut measured by qPCR at 6 days of induction.

(D) Relative expression of *dilp3* mRNA in *esg*^{ts}>*yki*^{act} midgut at 6 days of induction. *thread* (*th*) is a known transcriptional target of *yki*.

(E) Relative mRNA abundance of glycolytic enzymes in the midgut of *esg*^{ts}>*yki*^{act} flies at 8 days of induction.

(F) [U-^{14}C]glucose incorporation in the midgut (left) and whole-body void of midgut and hemolymph (right).

All qPCR values are mean ± SDs, and other measurements are mean ± SEMs. Transgenes are induced with *esg*^{ts} by shifting to the nonpermissive temperature (29°C). *p ≤ 0.05, Student's t test compared to control. Genotypes are as shown in Figure 4.

of *ImpL2* induction in the *yki*$^{S/A}$ tumors as compared to *scrib*^{1}/*Ras*^{V12} tumors.

Our results do not rule out the existence of an additional factor(s) contributing to the bloating syndrome and organ-wasting phenotypes. Indeed, the partial rescue of the bloating syndrome and organ-wasting phenotypes by depletion of *ImpL2* in *esg*^{ts}>*yki*^{act} midguts suggests the existence of an additional factor(s). Moreover, we observed that ectopic expression of *ImpL2* in ECs was not sufficient to reduce whole-body triglyceride and glycogen levels (data not shown), although it caused hyperglycemia, reduction of Akt1 phosphorylation, and increase of hemolymph volume (Figures S4G–S4J). Thus, given the involvement of diverse factors in the wasting process in mammals, it is likely that in addition to ImpL2, another factor(s) contributes to systemic organ wasting in *Drosophila*.

Our study shows that the bloating syndrome caused by *esg*^{ts}>*yki*^{act} is associated with *ImpL2*, as depletion of *ImpL2* from *esg*^{ts}>*yki*^{act} midguts significantly rescues the bloating phenotype. Given the observation that elevated expression of *ImpL2* from *esg*^{ts}>*yki*^{act} midgut induces hyperglycemia, we speculate that the accumulation of trehalose in hemolymph is a factor involved in bloating, because a high concentration of trehalose can cause water influx to adjust hemolymph osmolarity to physiological levels. Interestingly, recent findings have

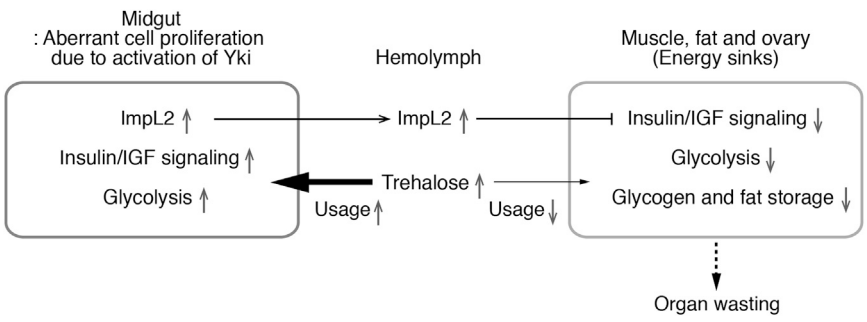

Figure 7. Model of the Tissue-Autonomous and Systemic Changes Caused by Aberrant Activation of Yki in ISCs

shown that disruption of *l(2)gl* in discs activates *yki* (Grzeschik et al., 2010; Halder and Johnson, 2011; Menéndez et al., 2010; Staley and Irvine, 2012), suggesting that the bloating syndrome observed in flies with transplanted *l(2)gl* mutant discs may be due to aberrant *yki* activity.

Our findings are reminiscent of a previous study showing that in *Drosophila*, humoral infection with the bacterial pathogen *Mycobacterium marinum*, which is closely related to *Mycobacterium tuberculosis*, causes a progressive loss of energy stores in the form of fat and glycogen—a wasting-like phenotype (Dionne et al., 2006). Similar to our observation, Dionne et al. found that infection with *M. marinum* caused a downregulation of Akt1 phosphorylation. Given our observation that *ImpL2* produced from $esg^{ts}>yki^{act}$ affects systemic insulin/IGF signaling, it will be of interest to test whether *ImpL2* expression is increased upon infection with *M. marinum* and mediates the effect on the loss of fat and glycogen storage.

yki plays critical roles in tissue growth, repair, and regeneration by inducing cell proliferation (Johnson and Halder, 2014; Pan, 2010; Staley and Irvine, 2012), a process requiring additional nutrients to support rapid synthesis of macromolecules including lipids, proteins, and nucleotides. In particular, increased aerobic glycolysis metabolizing glucose into lactate is a characteristic feature of many cancerous and normal proliferating cells (Vander Heiden et al., 2011). Interestingly, the aberrant activation of *yki* in ISCs caused a disparity in the gene expression of glycolytic enzymes and the activity of insulin/IGF signaling between the proliferating midgut and other tissues, such as muscle and ovaries (Figure 7). Thus, we speculate that this disparity favors Yki-induced cell proliferation by increasing the availability of trehalose/glucose to the proliferating midgut, which presumably requires high levels of trehalose/glucose (Figure 7). Additionally, it will be of interest to test whether activation of Yki during tissue growth, repair, and regeneration alters systemic metabolism in a similar manner.

EXPERIMENTAL PROCEDURES

Fly Stocks and Manipulation of Midgut Progenitor Cells

$UAS\text{-}yki^{act}$ (*w*;; UAS-yki.S111A.S168A.S250A.V5*; 228817) (Oh and Irvine, 2009) was obtained from the Bloomington *Drosophila* Stock Center. esg^{ts} refers to $tub\text{-}GAL80^{ts}$, *esg-GAL4*, *UAS-GFP* (II) (Apidianakis et al., 2009). RNAi line *15009R-3* against *ImpL2* was obtained from the National Institute of Genetics, Japan. *30931* is an RNAi line against *ImpL2* obtained from the Vienna *Drosophila* Resource Center, Austria. RNAi lines obtained from the Transgenic RNAi Project (http://www.flyrnai.org) are *JF01482* (*InR*), *JF01987* (*Pten*), and *HM04007* (*Akt1*). Additionally, we used *UAS-Pten* (III), *UAS-myr-Akt1* (III), and $ImpL2^{Def20}$ (gift from Hugo Stocker).

To induce transgenes in midgut stem cells, we followed the experimental procedures described previously (Apidianakis et al., 2009). Briefly, crosses were set up with esg^{ts} at room temperature, and after 3 days of incubation at room temperature were transferred to 18°C to activate $GAL80^{ts}$, thus restricting the expression of the Gal4-induced transgenes. Zero- to 4-day-old adult progenies were collected and placed at 29°C to induce the transgenes. Progenies from a cross between esg^{ts} and w^{1118} were used as controls. During incubation at 29°C, flies were transferred onto fresh food every 2 days.

Measurement of Carbohydrate and Triglyceride Levels

We measured fly carbohydrates and triglycerides as described previously (Song et al., 2010, 2014; Teleman et al., 2005). To prepare fly lysates for metabolic assays, we homogenized six female adults from each group in 400 μl PBS supplemented with 0.2% Triton X-100, heated the homogenate at 70°C for 5 min, and collected the supernatant after centrifugation at 14,000 rpm for 10 min. Whole-body trehalose levels were measured from 10 μl of supernatant treated with 0.2 μl trehalase (Megazyme; E-TREH) at 37°C for 30 min using glucose assay reagent (Megazyme; K-GLUC) following the manufacturer's protocol. We subtracted the amount of free glucose from the measurement and then normalized the subtracted values to protein levels in the supernatant. Whole-body glycogen levels were determined from 10 μl of supernatant preincubated with 1 μl amyloglucosidase (Sigma-Aldrich; A7420) at 37°C for 30 min using glucose assay reagent (Megazyme; K-GLUC). Free glucose levels were subtracted from the measurements, and glycogen levels were normalized to total protein levels. To measure whole-body triglycerides, we processed 10 μl of supernatant using a Serum Triglyceride Determination kit (Sigma-Aldrich; TR0100). We subtracted the amount of free glycerol in the supernatant from the measurement and then normalized the subtracted values to protein levels in the supernatant.

To measure circulating trehalose concentrations, hemolymph was extracted from 10–20 decapitated female adults by centrifugation at 1,500 × *g* for 15 min. Half a microliter of the collected hemolymph was diluted in 40 μl of TBS buffer (5 mM Tris-HCl [pH 6.6], 137 mM NaCl, 2.7 mM KCl), heated at 70°C for 5 min, and centrifuged at 14,000 rpm for 10 min. The supernatant was treated with 0.2 μl trehalase (Megazyme; E-TREH) at 37°C for 30 min and then used to measure circulating trehalose levels with glucose assay reagent (Megazyme; K-GLUC). We subtracted the amount of free glucose in the supernatant from the measurement.

Hemolymph volumes were measured using either a micropipette P2.5 (Eppendorf) or P10 (Gilson) and normalized to the number of flies used for hemolymph extraction.

Glucose Incorporation Assay

Fifteen to 25 flies incubated at 29°C for 3 days were transferred onto fresh food with 2 μCi [U-^{14}C]glucose (PerkinElmer; NEC042V). After 2 days of incubation at 29°C, the flies were transferred again onto fresh food with 2 μCi [U-^{14}C]glucose and incubated for an additional 2 days. To remove the food in the gut, we placed the flies onto nonradioactive food for 7–8 hr prior to dissection. Then, seven midguts were dissected in PBS and collected in 250 μl RIPA buffer (50 mM Tris-HCl [pH 7.4], 150 mM NaCl, 1% sodium deoxycholate, 1 mM EDTA, 0.1% SDS, 1% NP-40) after rinsing them twice with PBS. To collect the whole-body void of midgut and hemolymph, we dissected out the midguts through a small incision in the abdomen. Dissected flies were placed in an Eppendorf tube with 1 ml PBS and then washed four times with 1 ml PBS by inverting three to five times. Three dissected flies were homogenized in 250 μl RIPA buffer. After homogenization, we added 300 μl water to the homogenates to increase the volume. Five hundred microliters of homogenate was mixed with 10 ml Ultima Gold liquid scintillation cocktail (PerkinElmer; 6013326) in 20-ml glass scintillation vials. Disintegrations per minute values were measured and normalized to control.

RNA Sequencing Analysis of Muscle Transcriptome

To extract total RNAs for RNA sequencing (RNA-seq) experiments, we used ten thoraces dissected out from flies incubated for 8 days at 29°C. After assessing RNA quality with an Agilent Bioanalyzer, mRNAs were enriched by poly(A) pull-down. Then, sequencing libraries constructed with an Illumina TruSeq RNA preparation kit were sequenced using an Illumina HiSeq 2000 at the Columbia Genome Center (http://systemsbiology.columbia.edu/genome-center). We multiplexed samples in each lane, which yields a targeted number of single-end 100-bp reads for each sample, as a fraction of 180 million reads for the whole lane. Sequence reads were mapped back to the *Drosophila* genome (FlyBase genome annotation version r5.51) using TopHat (Trapnell et al., 2009). With the uniquely mapped reads, we quantified gene expression levels using Cufflinks (Trapnell et al., 2012) (fragments per kb of exon per million fragments mapped values). Next, we performed data normalization on the read counts and applied a negative binomial statistical framework using the Bioconductor package DESeq to quantify differential expression between experimental and control data. The RNA-seq data were deposited in the Gene Expression Omnibus (accession number GSE65325).

Metabolomics of Hemolymph Metabolites

To collect hemolymph, thoraces of approximately 200 flies were pierced with a tungsten needle. Next, the flies were placed in a perforated 0.5-ml Eppendorf tube within a 1.5-ml Eppendorf tube and then centrifuged twice at 2,348 × *g* for 4 min at 4°C with a gentle mixing of the flies between centrifugations. Collected hemolymph was centrifuged again at 2,348 × *g* for 3 min to precipitate hemocytes and other debris. The supernatant was centrifuged at 14,000 × *g* for 15 min to remove the insoluble fraction. Processed hemolymph was flash-frozen on dry ice and kept at −80°C until metabolomic sample preparation.

Metabolomic samples were prepared essentially as described previously (Yuan et al., 2012). Briefly, a hemolymph sample was diluted in −80°C methanol for a final methanol concentration of 80%. Then, the sample was briefly vortexed and stored at −80°C overnight. The sample was then centrifuged at 14,000 × *g* for 10 min. The supernatant was dried in a SpeedVac and then frozen at −80°C. For liquid chromatography-tandem mass spectrometry (LC-MS/MS), the resuspended sample in 20 μl of LC-MS-grade water was centrifuged and 10 μl was injected. Mass spectrometry was performed as described previously (Yuan et al., 2012) at the Beth Israel Deaconess Medical Center Mass Spectrometry Facility (http://www.bidmcmassspec.org). Briefly, selected reaction monitoring of 287 Q1/Q3 transitions was targeted in positive/negative switching mode using a 5500 QTRAP hybrid triple quadrupole mass spectrometer (AB SCIEX). Amide HILIC chromatography (Waters) was used at high pH over a 20-min gradient. Integrated peak area values of each metabolite were normalized to hemolymph volume or fly number.

ACCESSION NUMBERS

The accession number for the RNA-seq data reported in this paper is GEO: GSE65325.

SUPPLEMENTAL INFORMATION

Supplemental Information includes Supplemental Experimental Procedures, seven figures, and five tables and can be found with this article online at http://dx.doi.org/10.1016/j.devcel.2015.02.012.

ACKNOWLEDGMENTS

We thank the Transgenic RNAi Project, National Institute of Genetics (Japan), and Bloomington Drosophila Stock Center for fly stocks, Dr. Hugo Stocker for *ImpL2* stocks, and Drs. Stephanie Mohr, Richelle Sopko, Jonathan Zirin, Richard Binari, and Akhila Rajan for comments on the manuscript. We thank Alejandra Figueroa-Clarevega and David Bilder for exchange of information on the role of ImpL2 before publication. We also thank Min Yuan for help with the mass spectrometry experiments. Y.K. was supported in part by the Damon Runyon Cancer Research Foundation. This work was supported in part by P01-CA120964 (J.M.A. and N.P.) and R01-DK088718 (N.P.). N.P. is an Investigator of the Howard Hughes Medical Institute.

Received: September 28, 2014
Revised: December 17, 2014
Accepted: February 11, 2015
Published: April 6, 2015

REFERENCES

Alic, N., Hoddinott, M.P., Vinti, G., and Partridge, L. (2011). Lifespan extension by increased expression of the *Drosophila* homologue of the IGFBP7 tumour suppressor. Aging Cell *10*, 137–147.

Apidianakis, Y., Pitsouli, C., Perrimon, N., and Rahme, L. (2009). Synergy between bacterial infection and genetic predisposition in intestinal dysplasia. Proc. Natl. Acad. Sci. USA *106*, 20883–20888.

Benjamini, Y., and Hochberg, Y. (1995). Controlling the false discovery rate: a practical and powerful approach to multiple testing. J. R. Stat. Soc. Series B Stat. Methodol. *57*, 289–300.

Bodine, S.C., Stitt, T.N., Gonzalez, M., Kline, W.O., Stover, G.L., Bauerlein, R., Zlotchenko, E., Scrimgeour, A., Lawrence, J.C., Glass, D.J., and Yancopoulos, G.D. (2001). Akt/mTOR pathway is a crucial regulator of skeletal muscle hypertrophy and can prevent muscle atrophy in vivo. Nat. Cell Biol. *3*, 1014–1019.

Deboer, M.D. (2009). Animal models of anorexia and cachexia. Expert Opin. Drug Discov. *4*, 1145–1155.

Delano, M.J., and Moldawer, L.L. (2006). The origins of cachexia in acute and chronic inflammatory diseases. Nutr. Clin. Pract. *21*, 68–81.

Demontis, F., and Perrimon, N. (2010). FOXO/4E-BP signaling in *Drosophila* muscles regulates organism-wide proteostasis during aging. Cell *143*, 813–825.

Dionne, M.S., Pham, L.N., Shirasu-Hiza, M., and Schneider, D.S. (2006). Akt and FOXO dysregulation contribute to infection-induced wasting in *Drosophila*. Curr. Biol. *16*, 1977–1985.

Fearon, K.C., Glass, D.J., and Guttridge, D.C. (2012). Cancer cachexia: mediators, signaling, and metabolic pathways. Cell Metab. *16*, 153–166.

Fearon, K., Arends, J., and Baracos, V. (2013). Understanding the mechanisms and treatment options in cancer cachexia. Nat. Rev. Clin. Oncol. *10*, 90–99.

Figueroa-Clarevega, A., and Bilder, D. (2015). Malignant *Drosophila* tumors interrupt insulin signaling to induce cachexia-like wasting. Dev. Cell *33*, this issue, 47–55.

Gateff, E., and Schneiderman, H.A. (1974). Developmental capacities of benign and malignant neoplasms of *Drosophila*. Wilhelm Roux Arch. Entwickl. Mech. Org. *176*, 23–65.

Géminard, C., Rulifson, E.J., and Léopold, P. (2009). Remote control of insulin secretion by fat cells in *Drosophila*. Cell Metab. *10*, 199–207.

Greene, J.C., Whitworth, A.J., Kuo, I., Andrews, L.A., Feany, M.B., and Pallanck, L.J. (2003). Mitochondrial pathology and apoptotic muscle degeneration in *Drosophila* parkin mutants. Proc. Natl. Acad. Sci. USA *100*, 4078–4083.

Grzeschik, N.A., Parsons, L.M., Allott, M.L., Harvey, K.F., and Richardson, H.E. (2010). Lgl, aPKC, and Crumbs regulate the Salvador/Warts/Hippo pathway through two distinct mechanisms. Curr. Biol. *20*, 573–581.

Halder, G., and Johnson, R.L. (2011). Hippo signaling: growth control and beyond. Development *138*, 9–22.

Han, H.Q., Zhou, X., Mitch, W.E., and Goldberg, A.L. (2013). Myostatin/activin pathway antagonism: molecular basis and therapeutic potential. Int. J. Biochem. Cell Biol. *45*, 2333–2347.

Harvey, K.F., and Hariharan, I.K. (2012). The Hippo pathway. Cold Spring Harb. Perspect. Biol. *4*, a011288.

Hirabayashi, S., Baranski, T.J., and Cagan, R.L. (2013). Transformed *Drosophila* cells evade diet-mediated insulin resistance through Wingless signaling. Cell *154*, 664–675.

Honegger, B., Galic, M., Köhler, K., Wittwer, F., Brogiolo, W., Hafen, E., and Stocker, H. (2008). Imp-L2, a putative homolog of vertebrate IGF-binding protein 7, counteracts insulin signaling in *Drosophila* and is essential for starvation resistance. J. Biol. *7*, 10.

Ikeya, T., Galic, M., Belawat, P., Nairz, K., and Hafen, E. (2002). Nutrient-dependent expression of insulin-like peptides from neuroendocrine cells in the CNS contributes to growth regulation in *Drosophila*. Curr. Biol. *12*, 1293–1300.

Ja, W.W., Carvalho, G.B., Mak, E.M., de la Rosa, N.N., Fang, A.Y., Liong, J.C., Brummel, T., and Benzer, S. (2007). Prandiology of *Drosophila* and the CAFE assay. Proc. Natl. Acad. Sci. USA *104*, 8253–8256.

Johnson, R., and Halder, G. (2014). The two faces of Hippo: targeting the Hippo pathway for regenerative medicine and cancer treatment. Nat. Rev. Drug Discov. *13*, 63–79.

Karpowicz, P., Perez, J., and Perrimon, N. (2010). The Hippo tumor suppressor pathway regulates intestinal stem cell regeneration. Development *137*, 4135–4145.

Kir, S., White, J.P., Kleiner, S., Kazak, L., Cohen, P., Baracos, V.E., and Spiegelman, B.M. (2014). Tumour-derived PTH-related protein triggers adipose tissue browning and cancer cachexia. Nature *513*, 100–104.

Menéndez, J., Pérez-Garijo, A., Calleja, M., and Morata, G. (2010). A tumor-suppressing mechanism in *Drosophila* involving cell competition and the Hippo pathway. Proc. Natl. Acad. Sci. USA *107*, 14651–14656.

Murali, T., Pacifico, S., Yu, J., Guest, S., Roberts, G.G., III, and Finley, R.L., Jr. (2011). DroID 2011: a comprehensive, integrated resource for protein, transcription factor, RNA and gene interactions for *Drosophila*. Nucleic Acids Res. *39*, D736–D743.

O'Brien, L.E., Soliman, S.S., Li, X., and Bilder, D. (2011). Altered modes of stem cell division drive adaptive intestinal growth. Cell *147*, 603–614.

Oh, H., and Irvine, K.D. (2009). In vivo analysis of Yorkie phosphorylation sites. Oncogene *28*, 1916–1927.

Pan, D. (2010). The Hippo signaling pathway in development and cancer. Dev. Cell *19*, 491–505.

Penna, F., Minero, V.G., Costamagna, D., Bonelli, G., Baccino, F.M., and Costelli, P. (2010). Anti-cytokine strategies for the treatment of cancer-related anorexia and cachexia. Expert Opin. Biol. Ther. *10*, 1241–1250.

Planté-Bordeneuve, V., and Said, G. (2011). Familial amyloid polyneuropathy. Lancet Neurol. *10*, 1086–1097.

Puig, O., and Tjian, R. (2005). Transcriptional feedback control of insulin receptor by dFOXO/FOXO1. Genes Dev. *19*, 2435–2446.

Ren, F., Wang, B., Yue, T., Yun, E.Y., Ip, Y.T., and Jiang, J. (2010). Hippo signaling regulates *Drosophila* intestine stem cell proliferation through multiple pathways. Proc. Natl. Acad. Sci. USA *107*, 21064–21069.

Rommel, C., Bodine, S.C., Clarke, B.A., Rossman, R., Nunez, L., Stitt, T.N., Yancopoulos, G.D., and Glass, D.J. (2001). Mediation of IGF-1-induced skeletal myotube hypertrophy by PI(3)K/Akt/mTOR and PI(3)K/Akt/GSK3 pathways. Nat. Cell Biol. *3*, 1009–1013.

Sandri, M., Sandri, C., Gilbert, A., Skurk, C., Calabria, E., Picard, A., Walsh, K., Schiaffino, S., Lecker, S.H., and Goldberg, A.L. (2004). Foxo transcription factors induce the atrophy-related ubiquitin ligase atrogin-1 and cause skeletal muscle atrophy. Cell *117*, 399–412.

Shaw, R.L., Kohlmaier, A., Polesello, C., Veelken, C., Edgar, B.A., and Tapon, N. (2010). The Hippo pathway regulates intestinal stem cell proliferation during *Drosophila* adult midgut regeneration. Development *137*, 4147–4158.

Sloth Andersen, A., Hertz Hansen, P., Schaffer, L., and Kristensen, C. (2000). A new secreted insect protein belonging to the immunoglobulin superfamily binds insulin and related peptides and inhibits their activities. J. Biol. Chem. *275*, 16948–16953.

Song, W., Ren, D., Li, W., Jiang, L., Cho, K.W., Huang, P., Fan, C., Song, Y., Liu, Y., and Rui, L. (2010). SH2B regulation of growth, metabolism, and longevity in both insects and mammals. Cell Metab. *11*, 427–437.

Song, W., Veenstra, J.A., and Perrimon, N. (2014). Control of lipid metabolism by tachykinin in *Drosophila*. Cell Rep. *9*, 40–47.

Staley, B.K., and Irvine, K.D. (2012). Hippo signaling in *Drosophila*: recent advances and insights. Dev. Dyn. *241*, 3–15.

Subramanian, A., Tamayo, P., Mootha, V.K., Mukherjee, S., Ebert, B.L., Gillette, M.A., Paulovich, A., Pomeroy, S.L., Golub, T.R., Lander, E.S., and Mesirov, J.P. (2005). Gene set enrichment analysis: a knowledge-based approach for interpreting genome-wide expression profiles. Proc. Natl. Acad. Sci. USA *102*, 15545–15550.

Teleman, A.A., Chen, Y.W., and Cohen, S.M. (2005). 4E-BP functions as a metabolic brake used under stress conditions but not during normal growth. Genes Dev. *19*, 1844–1848.

Tisdale, M.J. (1997). Biology of cachexia. J. Natl. Cancer Inst. *89*, 1763–1773.

Tisdale, M.J. (2009). Mechanisms of cancer cachexia. Physiol. Rev. *89*, 381–410.

Trapnell, C., Pachter, L., and Salzberg, S.L. (2009). TopHat: discovering splice junctions with RNA-seq. Bioinformatics *25*, 1105–1111.

Trapnell, C., Roberts, A., Goff, L., Pertea, G., Kim, D., Kelley, D.R., Pimentel, H., Salzberg, S.L., Rinn, J.L., and Pachter, L. (2012). Differential gene and transcript expression analysis of RNA-seq experiments with TopHat and Cufflinks. Nat. Protoc. *7*, 562–578.

Vander Heiden, M.G., Cantley, L.C., and Thompson, C.B. (2009). Understanding the Warburg effect: the metabolic requirements of cell proliferation. Science *324*, 1029–1033.

Vander Heiden, M.G., Lunt, S.Y., Dayton, T.L., Fiske, B.P., Israelsen, W.J., Mattaini, K.R., Vokes, N.I., Stephanopoulos, G., Cantley, L.C., Metallo, C.M., and Locasale, J.W. (2011). Metabolic pathway alterations that support cell proliferation. Cold Spring Harb. Symp. Quant. Biol. *76*, 325–334.

Warburg, O. (1956). On the origin of cancer cells. Science *123*, 309–314.

Yang, X., and Xu, T. (2011). Molecular mechanism of size control in development and human diseases. Cell Res. *21*, 715–729.

Ye, X., Deng, Y., and Lai, Z.C. (2012). Akt is negatively regulated by Hippo signaling for growth inhibition in *Drosophila*. Dev. Biol. *369*, 115–123.

Yuan, M., Breitkopf, S.B., Yang, X., and Asara, J.M. (2012). A positive/negative ion-switching, targeted mass spectrometry-based metabolomics platform for bodily fluids, cells, and fresh and fixed tissue. Nat. Protoc. *7*, 872–881.

Zhang, W., Thompson, B.J., Hietakangas, V., and Cohen, S.M. (2011). MAPK/ERK signaling regulates insulin sensitivity to control glucose metabolism in *Drosophila*. PLoS Genet. *7*, e1002429.

Zinke, I., Kirchner, C., Chao, L.C., Tetzlaff, M.T., and Pankratz, M.J. (1999). Suppression of food intake and growth by amino acids in *Drosophila*: the role of pumpless, a fat body expressed gene with homology to vertebrate glycine cleavage system. Development *126*, 5275–5284.

Developmental Cell

Supplemental Information

Systemic Organ Wasting Induced by Localized Expression of the Secreted Insulin/IGF Antagonist *ImpL2*

Young Kwon, Wei Song, Ilia A. Droujinine, Yanhui Hu, John M. Asara, and Norbert Perrimon

Supplemental Figures

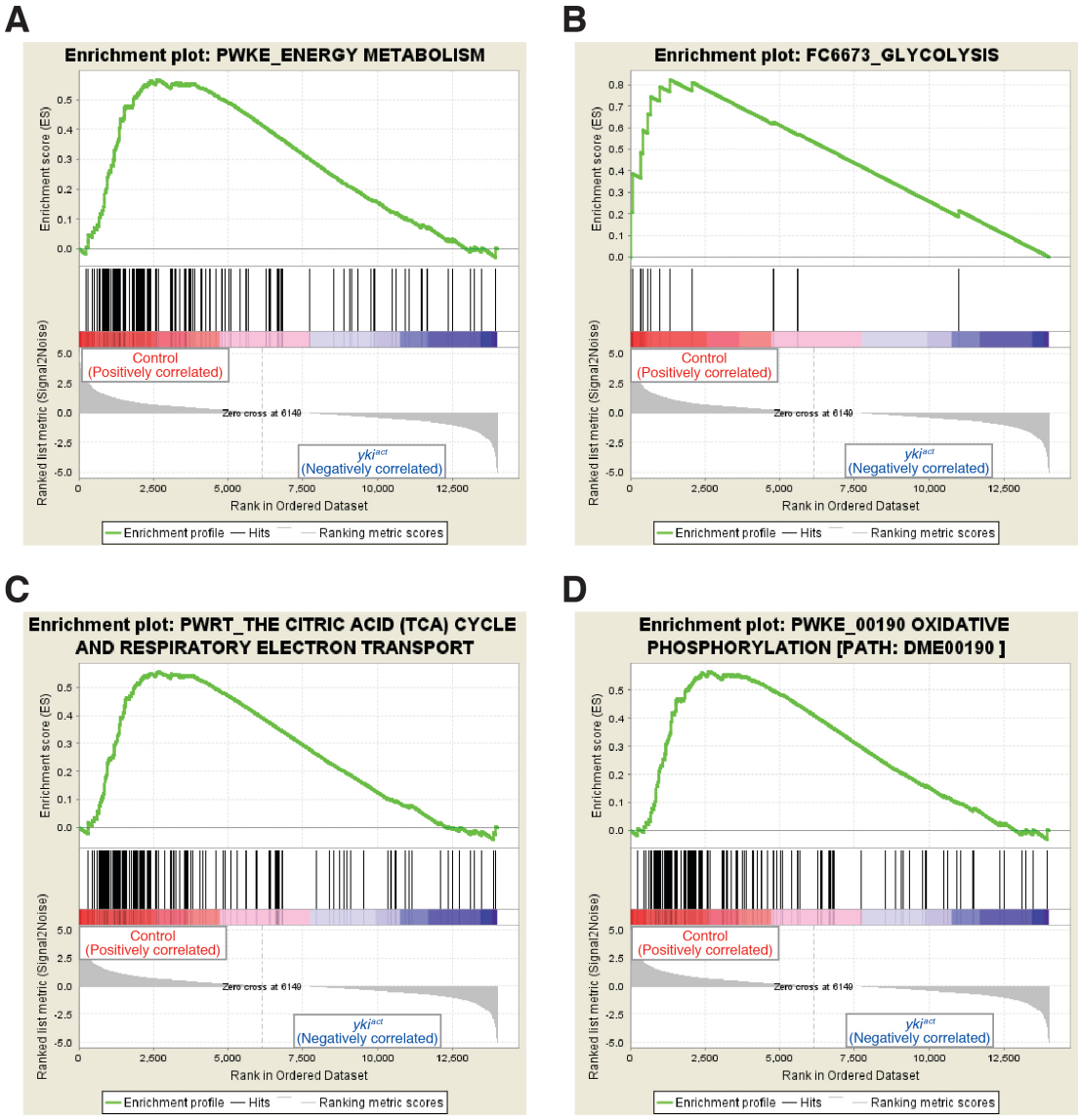

Figure S1. Representative GSEA plots showing repression of genes involved in energy metabolism in *esg^{ts}>yki^{act}* muscle transcriptome (related to Figure 2). (**A**) Energy metabolism (KEGG; normalized p value=0.000, GSEA). (**B**) Glycolysis (COMPLEAT; normalized p value=0.000, GSEA). (**C**) The citric acid (TCA) cycle and respiratory electron transport (Reactome; normalized p value=0.000, GSEA). (**C**) Oxidative phosphorylation (KEGG; normalized p value=0.000, GSEA). Additional information is shown in Table S4.

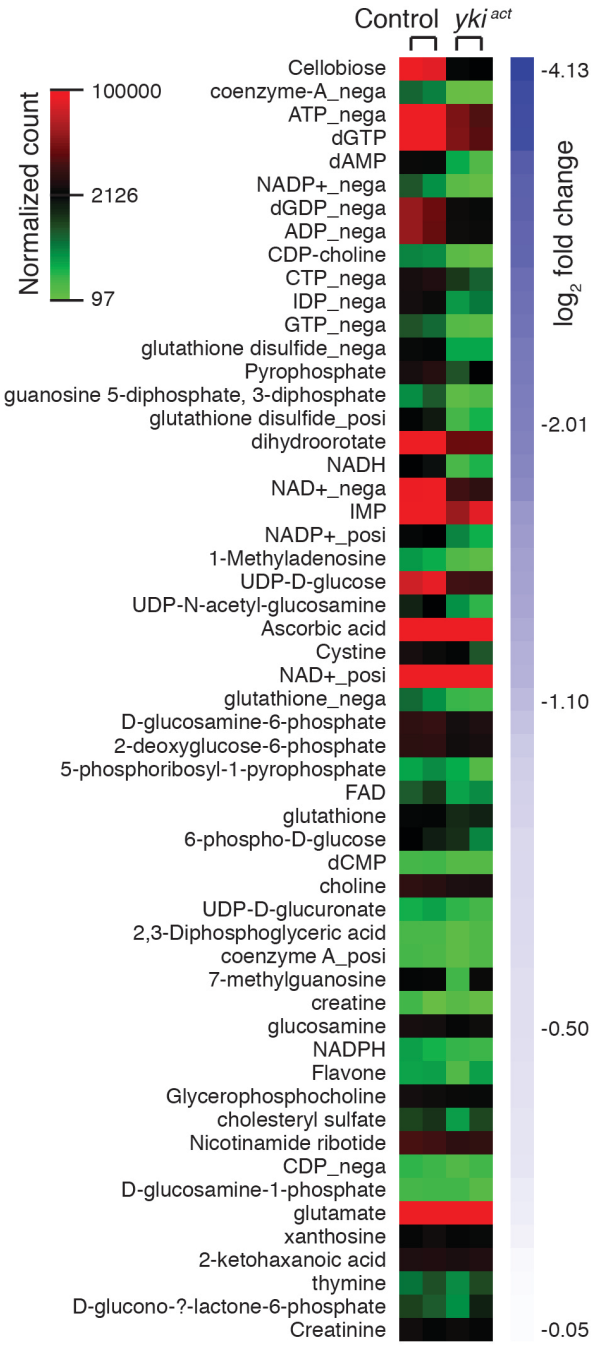

Figure S2. Reduced metabolites in hemolymph of *esg*^{ts}>*yki*^{act} flies (related to Figure 2). Heat map shows metabolite measurements of two experimental replicates of control and two experimental replicates of *esg*^{ts}>*yki*^{act}, which are normalized to the number of flies. Log_2 fold change values relative to control are indicated next to the heat map (blue bar).

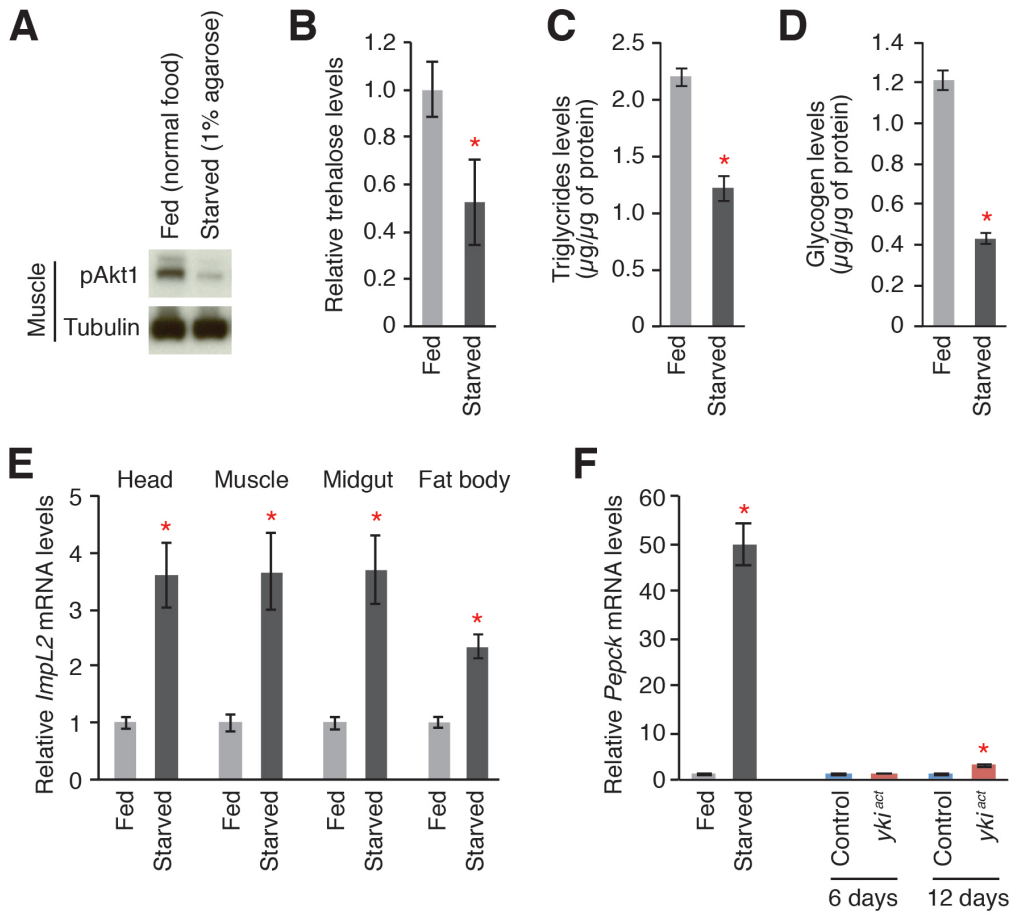

Figure S3. Characterization of starvation associated phenotypes (related to Figure 3). (**A**) Akt1 phosphorylation. (**B**) Whole body trehalose levels. Trehalose measurements are normalized to protein levels. (**C**) Whole body triglycerides levels. (**D**) Whole body glycogen levels. (**E**) Relative *ImpL2* mRNA expression. Relative values to controls are presented. (**F**) Relative *Pepck* mRNA expression. Genotypes of control is *esg-GAL4*, *tub-GAL80^{ts}*, *UAS-GFP*/+ and *yki^{act}* is *esg-GAL4*, *tub-GAL80^{ts}*, *UAS-GFP/+; UAS-yki^{act}/+*. Controls were fed on either normal food (Fed) or 1% agarose (Starved) for 24 hours. All measurements shown are mean±SDs. *p≤0.05 (Student's *t*-test) compared to control.

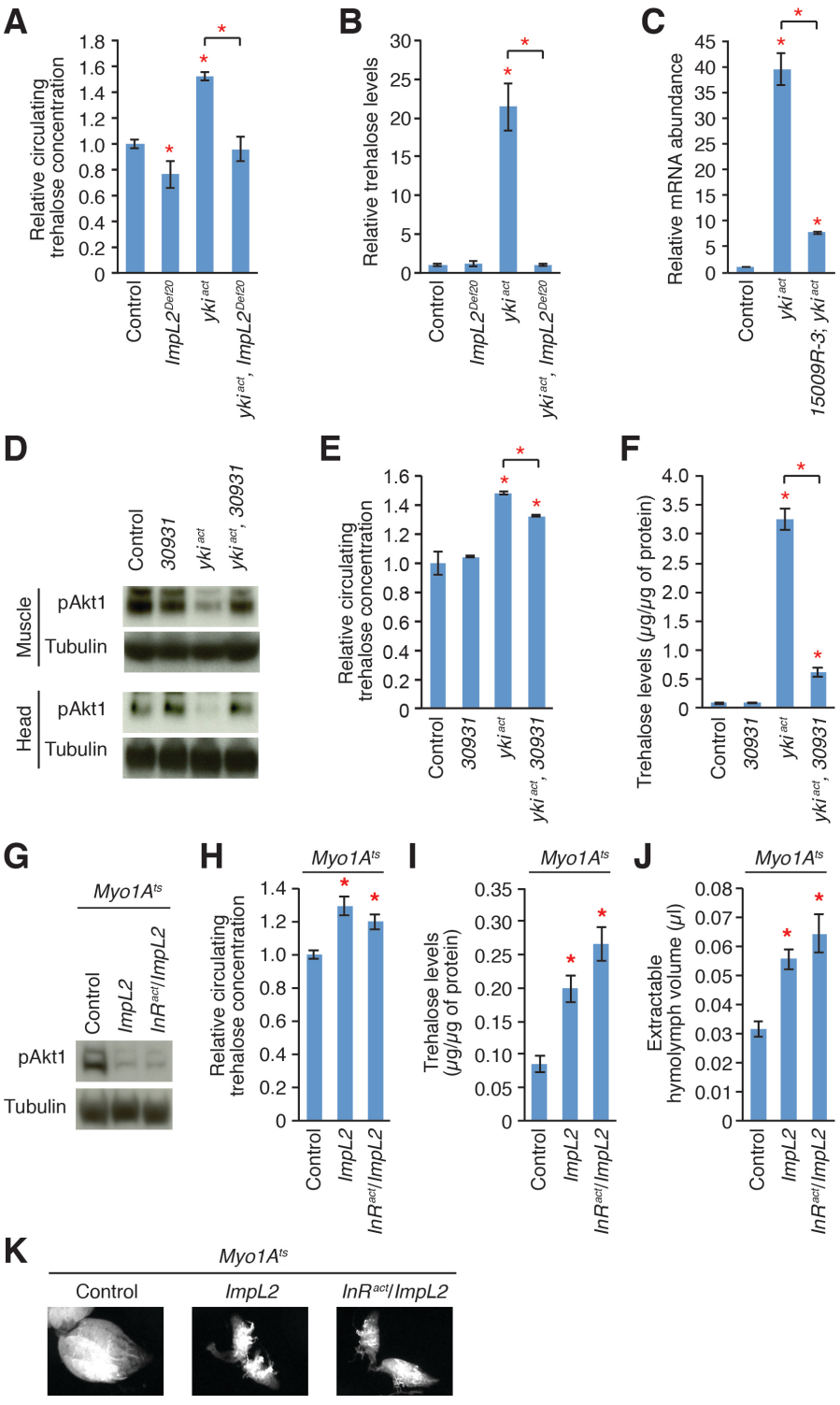

Figure S4. Further characterization of the role of ImpL2 (related to Figure 4). (**A-B**) Rescue of hyperglycemia associated with *esg*^{ts}>*yki*^{act} by *ImpL2*^{Def20}. Transgenes are induced with *esg*^{ts}. (**A**) Circulating trehalose concentrations at 8 days of induction. (**B**)

Relative trehalose levels in whole-body at 8 days of induction. Trehalose measurements are normalized to total protein amounts. (**C**) Relative expression levels of *ImpL2* in the midgut following expression of an *ImpL2*-RNAi line, *15009R-3* (NIG) with esg^{ts}. Expression levels are measured by qPCR. Values shown are mean±SDs. (**D-F**) Rescue of hyperglycemia and reduction of insulin/IGF signaling associated with $esg^{ts}>yki^{act}$ by depletion of *ImpL2* with an additional *ImpL2*-RNAi line, *30931*. Transgenes are induced with esg^{ts}. (**D**) Akt1 phosphorylation (pAkt1) in muscle and head at 8 days of induction. (**E**) Circulating trehalose concentrations at 8 days of induction. (**F**) Trehalose levels in whole-body at 8 days of induction. Measurements are normalized to total protein amounts. *30931* is an RNAi line against *ImpL2* obtained from VDRC. Genotypes in (**A-F**) are as follows: control is *esg-GAL4*, $tub\text{-}GAL80^{ts}$, *UAS-GFP*/+, yki^{act} is *esg-GAL4*, $tub\text{-}GAL80^{ts}$, *UAS-GFP*/+; $UAS\text{-}yki^{act}$/+, *30931* is *esg-GAL4*, $tub\text{-}GAL80^{ts}$, *UAS-GFP*/+; *30931*/+, yki^{act}, *30931* is *esg-GAL4*, $tub\text{-}GAL80^{ts}$, *UAS-GFP*/+; *30931,* $UAS\text{-}yki^{act}$/+, and other genotypes are as shown in Figure 4. (**G-K**) Systemic phenotypes induced by ectopic expression of *ImpL2* in midgut enterocytes. Transgenes are induced with $tub\text{-}Gal80^{ts}$; *Myo1A-GAL4*, *UAS-GFP* ($Myo1A^{ts}$) by shifting to 29°C. To avoid a direct effect on enterocytes caused by overexpression of *ImpL2*, we also combined an active form of the *Insulin-like receptor* (InR^{act}) (Wittwer et al., 2005), whose expression provides a cell-autonomous protection from the action of *ImpL2*. (**G**) Akt1 phosphorylation in muscle. Expression of *ImpL2* with or without InR^{act} decreased Akt1 phosphorylation in muscles. (**H**) Circulating trehalose concentrations. (**I**) Trehalose levels in whole-body. (**J**) Hemolymph volumes extractable from whole-flies. (**K**) Images of ovary at 8 days of induction. Overexpression of either *ImpL2* alone or together with an active form of *InR* (InR^{act}) in enterocytes causes ovary atrophy. All metabolic assay results shown are mean±SEMs. *p≤0.05 (Student's *t*-test) compared to control unless indicated with a bracket.

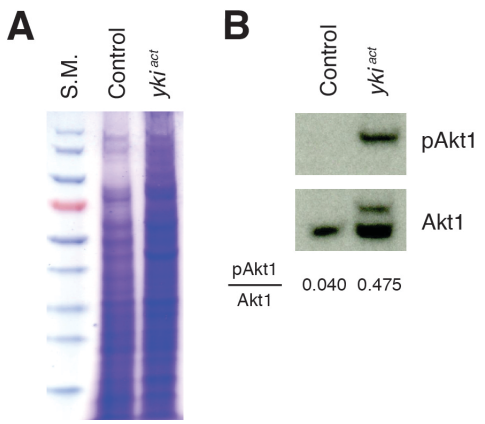

Figure S5. Measurement of Akt1 phosphorylation in the midgut (related to Figure 6). (A) Coomassie staining of the protein extracts from midgut. Protein extracts of five midguts from each genotype were run on SDS-PAGE gel, then stained with Coomassie brilliant blue. (**B**) Detection of phospho-Akt1 (pAkt1) and Akt1 by western blotting. Transgenes are induced with *esg*^{ts} for 6 days. Genotypes of control is *esg-GAL4*, *tub-GAL80*^{ts}, *UAS-GFP*/+ and *yki*^{act} is *esg-GAL4*, *tub-GAL80*^{ts}, *UAS-GFP*/+*; UAS-yki*^{act}/+.

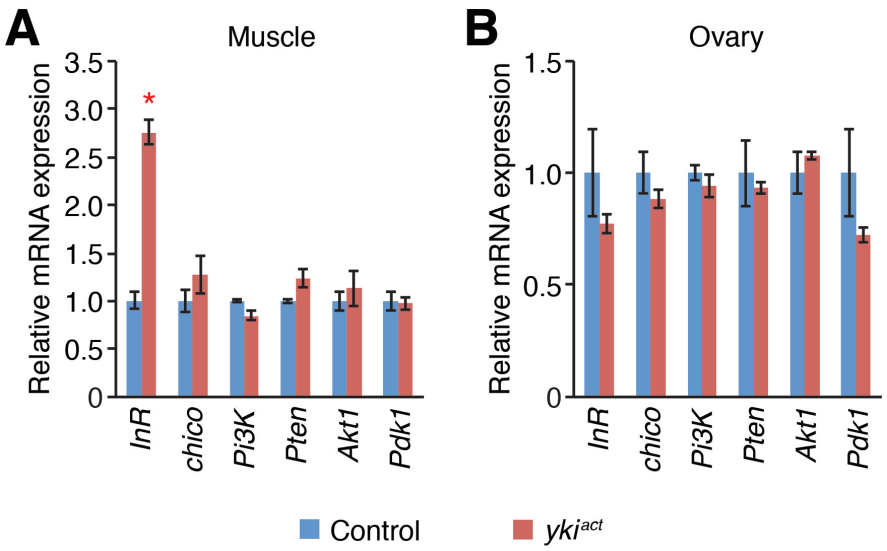

Figure S6. Relative mRNA abundance of insulin/IGF pathway components in muscle (A) and ovary (B) (related to Figure 6). Transgenes were induced for 6 days with *esg*^{ts}. Values shown are mean±SDs. *p<0.05, unpaired Student's *t*-test.

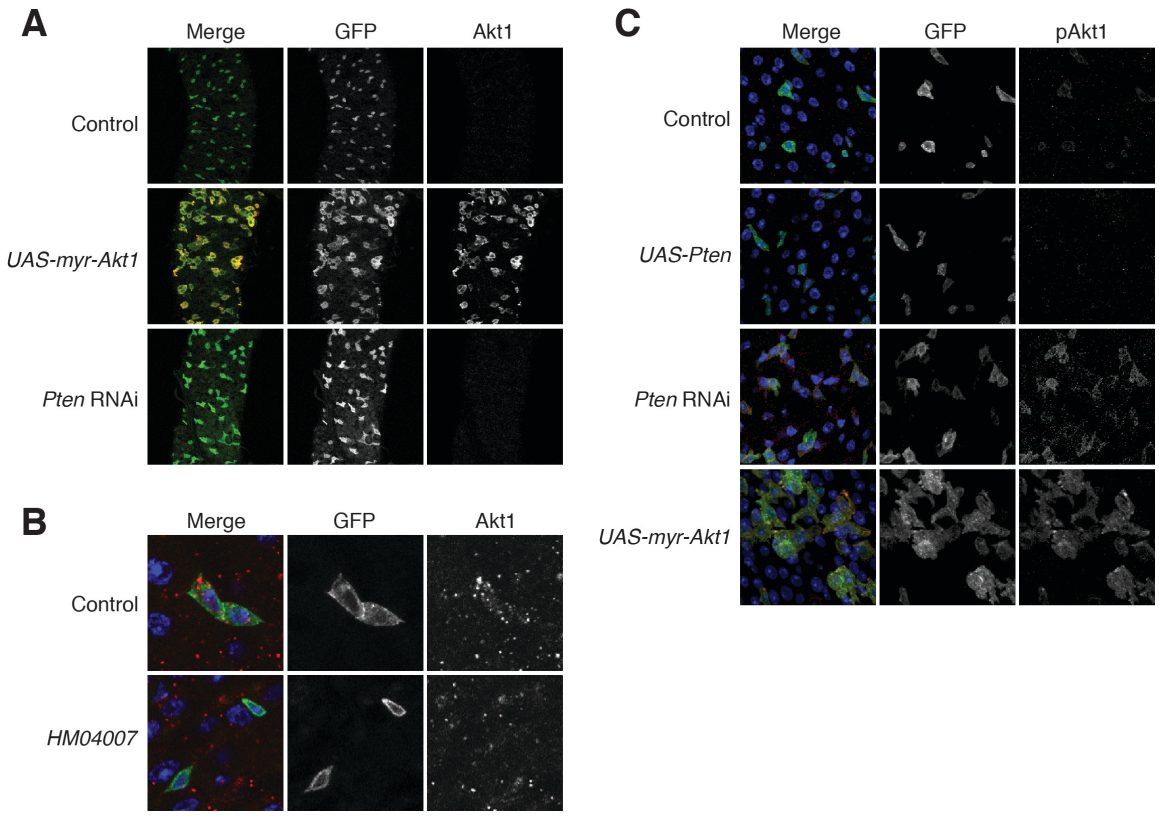

Figure S7. Characterization of anti-Akt and anti-phospho-*Drosophila* Akt antibodies in the midgut (related to Figure 6). (**A**) Detection of Akt1. Overexpression of myr-Akt1, but not activation of Akt1 by knockdown of *Pten*, specifically enhanced the fluorescent signal detected with the anti-Akt antibody (red in merge). GFP (green in merge) marks the midgut progenitor cells. Transgenes were induced for 6 days. (**B**) Detection of Akt1. Knockdown of *Akt1* with the RNAi line *HM04007* (TRiP) reduced basal Akt1 signal (red in merge) in the stem cells (GFP; green in merge). Akt1 signal is slightly enriched in stem cells (upper panels). Transgenes were induced for 6 days. (**C**) Detection of phospho-Akt1 (pAkt1; red in merge). Overexpression of *Pten* decreased pAkt1 signal, but knockdown of *Pten* or overexpression of *myr-Akt1* increased pAkt1 signal. Transgenes were induced with esg^{ts} for 10 days.

Supplemental Tables

Table S1. Muscle RNA-Seq results (related to Figure 2). Normalized values are shown.

Table S2. Gene list enrichment analysis of the muscle transcriptome of *esg^{ts}>yki^{act}* flies (related to Figure 2). (**A**) List of downregulated genes. (**B**) List of upregulated genes. (**C**) Selected gene sets enriched in downregulated transcriptome. (**D**) Selected gene sets enriched in upregulated transcriptome.

Table S3. Network of metabolic processes enriched in the downregulated muscle transcriptome of *esg^{ts}>yki^{act}* flies (related to Figure 2). The network is shown in Figure 2A.

Table S4. GSEA results of energy metabolism (related to Figure 2). A few selected pathways involved in energy metabolism are analyzed with GSEA program (Broad Institute) (Subramanian et al., 2005).

Table S5. Metabolomics of hemolymph metabolites (related to Figure 2). Normalized values to fly number (**A**) and hemolymph volume (**B**) are shown.

Supplemental Experimental Procedures

Immunostaining of the midgut

Prior to dissection, flies were fed on 4% sucrose for ~4 hours to remove food from the midgut. Midguts were dissected in PBS and stained overnight with anti-Akt antibody (Cell Signaling Technology, 9272; 1:200) or anti-phospho *Drosophila* Akt (Ser505, correspond to Ser473 in human) antibody (Cell Signaling Technology, 4054; 1:200) in PBS with 0.1% BSA, 0.3% Triton X-100 and 5% Normal Donkey Serum. Stainings were visualized with Alexa Fluor® 594 Donkey anti-rabbit IgG (Life Technologies). Maximum projections of 4-6 stacks of images across an epithelial layer were taken with a Leica TCS SP2-AOBS confocal microscope. We characterized the anti-Akt and anti-phospho-*Drosophila* Akt (Ser505) antibodies in the midgut since they were not previously used to stain Akt1 and pAkt1 in this tissue (Figure S7).

Additionally, we detected Akt1 or pAkt1 in the midgut by Western blot using the same antibodies. To inhibit proteases and phosphatases in the midgut, we homogenized 20 midguts directly in 2XSDS-PAGE sample buffer supplemented with 2 mM Benzamidine, 1 μM Pepsistatin, 1 mM PMSF, Protease inhibitor cocktail (Sigma) and Phosphatase inhibitor cocktail 1, 2 (Sigma). We ran the protein extracts corresponding to 5 midguts on SDS-PAGE. We tested protein amounts by Coomassie brilliant blue staining.

Quantification of mRNA expression

Total RNA was extracted from 15 midguts, 10 heads, 6 thoraces or 8 ovaries using TRIzol® reagent (Invitrogen, 15596-026). We synthesized first strand cDNA with 1 μg of total RNA using iScript™ Reverse Transcription Supermix (BIO-RAD, 170-8841) and performed quantitative PCR with CFX96 Real-Time System (BIO-RAD) using iQ™ SYBR Green Supermix (BIO-RAD, 170-8882). All expression values were normalized to *RpL32* (also known as *rp49*). All assays were performed in triplicate, and representative results are shown. The primer sequences used for quantitative PCR are as follows:
ImpL2, AAGAGCCGTGGACCTGGTA, TTGGTGAACTTGAGCCAGTCG;
InR, AAGCGTGGGAAAATTAAGATGGA, GGCTGTCAACTGCTTCTACTG;

chico, GCGCACTCACCTTATGACCA, GCACACGAATGTCAGGGATTT;
Pi3K, AGCCCAAGTATGAGACACCG, AACAGGCAGATTAGGTCCACC;
Pten, TCAGAAACCGTCTGGAAGATGT, CGCTCCGAGCATAGGTTATAGA;
Akt1, CCCAGCGTTACATCGGGTC, GCTCGCCCCTCTTCATCAG;
Pdk1, GTTCCCGGCTTCGTAAACCT, GCGGTTGATGTATGGCAACA;
th, GCTGGACTGGCTGGATAAAC, GCCGCAGAAAAAGCATTTAACT;
Hex-A, CTGCTTCTAACGGACGAACAG, GCCTTGGGATGTGTATCCTTGG;
Hex-C, GCGGAGGTGCGAGAACTTAT, CCACTTCCAGGCAAAAGCGA;
Pfk, CGAGCCTGTGTCCGTATGG, AGTTGGCTTCCTGGATGCAG;
Ald, GCCCAGAAAATCGTTGCCC, GGGTCAGTGCTGAACAACAG;
GAPDH, CCAATGTCTCCGTTGTGGA, TCGGTGTAGCCCAGGATT;
Eno, CGATCAAGGCCCGTCAAATCT, CCAGGGTGTCGTTCACATGG;
Pyk, GCAGGAGCTGATACCCAACTG, CGTGCGATCCGTGAGAGAA;
ImpL3, CAGCACGGCTCCAACTTTCT, GATGATGTTCTTGAGGATGTCGG;
Dilp2, ATGAGCAAGCCTTTGTCCTTC, ACCTCGTTGAGCTTTTCACTG;
Dilp3, ATGGGCATCGAGATGAGGTG, CGTTGAAGCCATACACACAGAG;
Dilp5, CGCTCCGTGATCCCAGTTC, AGGCAACCCTCAGCATGTC;
RpL32, GCTAAGCTGTCGCACAAATG, GTTCGATCCGTAACCGATGT;
Pepck, GAACTGACGGACTCTGCTTAC, GGTGCGTTCGGGATCACAA.

CAFE Assay

The CAFE assay was performed as previously described (Demontis and Perrimon, 2010; Ja et al., 2007). Briefly, 5 female flies deprived from food for 6 hours were provided with liquid food (5% yeast and 10% sucrose) maintained in 10 μl calibrated glass micropipettes. The amount of liquid food consumed was measured after incubating 10 hours.

Blue dye excretion assay

To measure food excretion rate, we fed flies with fresh food containing 2.5% (w/v) blue food dye (F D & C Blue Dye no. 1) overnight. Then, we divided the flies into two groups. One group of flies (Group A) was kept at -20°C, and the other group of flies

(Group B) was transferred onto normal food without dye. After incubating for 4 hours, flies were homogenized in 200 μl PBS. The amount of blue dye in supernatant was measured using a spectrophotometer. We calculated food excretion rate by {(blue dye amount from Group A) – (blue dye amount from Group B)} / (blue dye amount from Group A).

Dilp2 immunostaining

Dissected adults brains were fixed for 15 minutes in 4% formaldehyde. After fixation, the brains were stained overnight at 4°C with anti-dILP2 antibody (gift from Dr. Linda Partridge, University College London; 1:5000) in PBS with 0.1% BSA, 0.3% Triton X-100 and 5% Normal Donkey serum. Alexa Fluor® 594 Donkey anti-rabbit IgG (Life Technologies) was used to detect the staining. Confocal images were obtained using a Leica TCS SP2 AOBS system.

Measuring enzymatic activities in muscle

Hexokinase and Pyruvate Kinase activities in adult *Drosophila* muscle were measured using Hexokinase Colorimetric Assay Kit (Sigma-Aldrich, MAK091) and Pyruvate Kinase Activity Assay Kit (Sigma-Aldrich, MAK072) following manufacturer's protocols. Briefly, 6 thoraces were homogenized in 100 μl Hexokinase assay buffer or Pyruvate kinase assay buffer provided with the kits. After centrifugation at 14,000 rpm for 15 min at 4°C, supernatants were collected. The collected lysates were diluted 1:10 for Hexokinase assay and 1:100 for Pyruvate Kinase assay, and then 10 μl of diluted lysates were mixed with 50 μl Reaction Mixture. The measured values (Vmax) were normalized to lysate protein levels.

ATP measurement in thorax

6 thoraces were homogenized in 100 μl extraction buffer (6 M Guanidine Chloride, 100 mM Tris-HCl pH8.0, 4 mM EDTA), heated at 70°C for 5 minutes, then centrifuged at 14,000 rpm for 10 minutes at 4°C to remove cuticle and cell debris. ATP levels were measured using ATP Determination Kit (Invitrogen, A22066) following the

manufacturer's protocol and normalized to protein levels.

Electron Microscopy

We fixed thoraces in 0.1 M sodium cacodylate buffer (pH 7.4) containing 2.5% glutaraldehyde, 2% paraformaldehyde for overnight. The fixed samples were washed in 0.1M cacodylate buffer, fixed again with 1% osmiumtetroxide (OsO_4) and 1.5% potassium ferrocyanide ($KFeCN_6$) for 1 hour, and washed 3 times in water. Then, the samples were incubated in 1% aqueous uranyl acetate for 1 hour and followed by 2 washes in water and subsequent dehydration in grades of alcohol. The samples were then put in propyleneoxide for 1 hour and embedded in TAAB Epon (Marivac Canada Inc.).

Ultrathin sections (about 60nm) were cut on a Reichert Ultracut-S microtome, picked up on to copper grids, and then stained with lead citrate. The sections were examined in a JEOL 1200EX Transmission electron microscope, and images were recorded with an AMT 2k CCD camera.

Gene list enrichment analysis

For each gene, we calculated 4 combinatorial fold-change values relative to control using the DESeq normalized expression values for each gene from two control muscles and two $esg^{ts}>yki^{act}$ muscles RNA-Seq results. We selected genes as differentially expressed genes (upregulated or downregulated genes) if at least 3 out of these 4 combinatorial absolute $\log_2$ fold-change values were 1 or higher. Consequently, we identified 645 upregulated genes (4.6% of entire transcriptome) and 749 downregulated genes (5.3% of entire transcriptome) in the $esg^{ts}>yki^{act}$ muscles compared to control muscles (Table S1 and S2).

For gene list enrichment analysis, we first assembled gene lists, including pathways, complexes and target gene sets of transcription factors, from various public resources such as Gene Ontology (http://www.geneontology.org/), KEGG (Ogata et al., 1999), BioCarta (http://www.biocarta.com/), FlyReactome (http://fly.reactome.org/), DroID (Murali et al., 2011), COMPLEAT (Vinayagam et al., 2013) and Reactome (Croft et al., 2014). The gene lists from other species were converted into *Drosophila* gene lists

using an orthologous mapping tool DIOPT (Hu et al., 2011) with the least stringent filter setup. We performed enrichment analysis with up- and down-regulated muscle transcriptomes separately. Enrichment p values of gene lists were calculated using hyper-geometric distribution, and selected gene lists with p value less than 0.05 were presented (Table S2). Additionally, we analyzed a few selected metabolic pathways using GSEA program (Subramanian et al., 2005) (http://www.broadinstitute.org/gsea/index.jsp).

Supplemental References

Croft, D., Mundo, A.F., Haw, R., Milacic, M., Weiser, J., Wu, G., Caudy, M., Garapati, P., Gillespie, M., Kamdar, M.R.*, et al.* (2014). The Reactome pathway knowledgebase. Nucleic Acids Res *42*, D472-477.

Demontis, F., and Perrimon, N. (2010). FOXO/4E-BP signaling in Drosophila muscles regulates organism-wide proteostasis during aging. Cell *143*, 813-825.

Hu, Y., Flockhart, I., Vinayagam, A., Bergwitz, C., Berger, B., Perrimon, N., and Mohr, S.E. (2011). An integrative approach to ortholog prediction for disease-focused and other functional studies. BMC Bioinformatics *12*, 357.

Ja, W.W., Carvalho, G.B., Mak, E.M., de la Rosa, N.N., Fang, A.Y., Liong, J.C., Brummel, T., and Benzer, S. (2007). Prandiology of Drosophila and the CAFE assay. Proc Natl Acad Sci U S A *104*, 8253-8256.

Murali, T., Pacifico, S., Yu, J., Guest, S., Roberts, G.G., 3rd, and Finley, R.L., Jr. (2011). DroID 2011: a comprehensive, integrated resource for protein, transcription factor, RNA and gene interactions for Drosophila. Nucleic Acids Res *39*, D736-743.

Ogata, H., Goto, S., Sato, K., Fujibuchi, W., Bono, H., and Kanehisa, M. (1999). KEGG: Kyoto Encyclopedia of Genes and Genomes. Nucleic Acids Res *27*, 29-34.

Subramanian, A., Tamayo, P., Mootha, V.K., Mukherjee, S., Ebert, B.L., Gillette, M.A., Paulovich, A., Pomeroy, S.L., Golub, T.R., Lander, E.S.*, et al.* (2005). Gene set enrichment analysis: a knowledge-based approach for interpreting genome-wide expression profiles. Proc Natl Acad Sci U S A *102*, 15545-15550.

Vinayagam, A., Hu, Y., Kulkarni, M., Roesel, C., Sopko, R., Mohr, S.E., and Perrimon, N. (2013). Protein complex-based analysis framework for high-throughput data sets. Sci Signal *6*, rs5.

Wittwer, F., Jaquenoud, M., Brogiolo, W., Zarske, M., Wustemann, P., Fernandez, R., Stocker, H., Wymann, M.P., and Hafen, E. (2005). Susi, a negative regulator of Drosophila PI3-kinase. Dev Cell *8*, 817-827.